assumes only a bistable jump by 180°, other internal motions such as rotations by other angles, free rotations, vibrations, and distortions can also occur in a molecule. These need detailed calculations using numerical methods like molecular mechanics and Monte Carlo simulation.

In NOE calculations involving more than two spins, the cross-correlation between the different dipolar vectors often plays a significant role.[45] When an internal motion is also present apart from the overall motion, the cross-correlation spectral density functions have additional information about the correlation between the two motions. The present model assumes that the global and segmental motions are independent of each other, hence multispin NOE have been calculated in this paper by neglecting the cross-correlation effects.

Acknowledgment. Discussions with Prof. B. D. Nageswara Rao and Prof. P. Balaram, who also provided the peptide sample, are gratefully acknowledged. We thank Profs. C. L. Khetrapal and J. Tropp for perusal of the manuscript. A.K. acknowledges the Department of Science and Technology, India, for a research grant and V.V.K. acknowledges CSIR for a senior research fellowship.

Appendix: Direction Cosines of the Dipolar Vector in the Internal Frame

The coordinates of the nucleus D (tip of the vector $\bar{r}_I$) at any time t in the $S_I(X_I,Y_I,Z_I)$ are

$$x_I(t) = r_I \sin\beta \cos\alpha(t) \qquad y_I(t) = r_I \sin\beta \sin\alpha(t)$$
$$z_I(t) = r_I \cos\beta \tag{A1}$$

where α is the azimuthal of the $\bar{r}_I$ vector as shown in Figure 6. Consider a frame of reference $S'_C(X'_C,Y'_C,Z'_C)$, the same as the reference frame of convenience $S_C(X_C,Y_C,Z_C)$ except the origin is shifted from atom A to C where S_C is the frame of convenience with the origin at atom A as defined in Figure 1. The frame of convenience is taken such that the X_I and Z_I axes are in the same plane as the X'_C and Z'_C axes and the two Y axes are 180° out of phase (Figure 6). The transformation from S'_C to S_I is given by

$$\begin{bmatrix} x'_C(t) \\ y'_C(t) \\ z'_C(t) \end{bmatrix} = \begin{bmatrix} -\cos\Delta & 0 & \sin\Delta \\ 0 & -1 & 0 \\ \sin\Delta & 0 & \cos\Delta \end{bmatrix} \begin{bmatrix} x_I(t) \\ y_I(t) \\ z_I(t) \end{bmatrix} \tag{A2}$$

where Δ is the angle between the Z_I and the Z'_C or equivalently in terms of the geometry of the molecular fragment, given by $(\angle ABC) - \pi/2$. On translating the origin from atom C to A the coordinates of nucleus D in the frame S_C are

$$x_C(t) = r_{AB} + r_{BC} \sin\Delta + x'_C(t) \qquad y_C(t) = y'_C(t)$$
$$z_C(t) = r_{BC} \cos\Delta + z'_C(t) \tag{A3}$$

eqs 12-15 in the text are obtained by substituting eqs A1 and A2 in eq A3.

(45) (a) Krishnan, V. V.; Anil Kumar *J. Magn. Reson.* **1991**, *92*, 293-311. (b) Dalvit, C.; Bodenhausen, G. *Adv. Magn. Reson.* **1990**, *14*, 1-33.

Solution Structure of a Synthetic N-Glycosylated Cyclic Hexapeptide Determined by NMR Spectroscopy and MD Calculations†

H. Kessler,* H. Matter, G. Gemmecker, A. Kling, and M. Kottenhahn

Contribution from the Organisch-Chemisches Institut, Technische Universität München, Lichtenbergstrasse 4, D-8046 Garching, Germany. *Received January 17, 1991*

Abstract: The synthesis and conformational analysis by NMR spectroscopy and MD calculations of the N-glycosylated cyclic hexapeptide cyclo(-D-Pro-Phe-Ala-[*N*-2-acetamido-2-desoxy-β-D-glucopyranosyl)]Gln-Phe-Phe-) (I) and the cyclic hexapeptide precursor cyclo(-D-Pro-Phe-Ala-Glu(OtBu)-Phe-Phe-) (II) were carried out to study the influence of N-glycosylation on conformation of peptides. For both compounds, all of the distance constraints derived from 2D NOE measurements could not be satisfied by one conformation. Therefore, second conformers interconverting fast compared to the NMR time scale are assumed. The two conformations differ in the β-turn structure between Ala[3] and Phe[6] (βII- or βI-turns, respectively). The βII'-turn about amino acids D-Pro[1] and Phe[2] is highly conserved in both MD simulations. The conformations were refined by using restrained MD simulations in vacuo and in water. Additional MD simulations with application of time-dependent distance constraints provide further information about the internal flexibility of I. The conformational equilibrium could be confirmed; several conformational changes were detected evidenced by a large number of torsion angle fluctuations during the time scale of the simulation. Both proposed backbone conformers were significantly populated. The averaging over coupling constants and NOE data reveal the high flexibility of the structure and the good agreement with experimental data for both I and II. The N-glycosylation does not affect the conformation or the overall shape of the peptide backbone or side chains. It has no influence on the hydrogen-binding pattern or on the fast dynamical equilibrium of the molecule.

Introduction

Carbohydrates and glycoproteins are of great importance in biological recognition phenomena.[1] Therefore, the interest in the synthesis and conformations of glycopeptides as partial structures of glycoproteins has increased considerably.[2] Many applications for glycopeptides are currently being established, e.g., in the development of selective pharmaceuticals and for the improvement of pharmacokinetic properties.[3]

Presently, very little is known about the mutual conformational influences between the protein or peptide structures and the

†Abbreviations: BOC, *tert*-butoxycarbonyl; COLOC, heteronuclear correlation via long-range couplings; DQF-H,H-COSY, double quantum filtered proton-correlated spectroscopy; E.COSY, exclusive correlated spectroscopy; EDCI,*N*-ethyl-*N'*-[(dimethylamino)propyl]carbodiimide hydrochloride; HMBC, heteronuclear multiple bond correlation; HMQC, heteronuclear multiple quantum coherence correlation; HOBt, 1-hydroxybenzotriazole; solvent A, *n*-butanol/H_2O/acetic acid (3:1:1); solvent B, chloroform/methanol (9:1); solvent C, chloroform/methanol/acetic acid (95:5:3); NOE, nuclear Overhauser effect; NOESY, nuclear Overhauser and exchange spectroscopy; ROE, rotating frame NOE; ROESY, rotating frame Overhauser and exchange spectroscopy; TOCSY, total correlation spectroscopy; Z, benzyloxycarbonyl.

(1) (a) Feizi, T. *Nature* **1985**, *314*, 53-57. (b) Goldstein, E. J. Carbohydrate Protein Interaction. *ACS Symp. Ser.* **1979**, *No. 88*.

(2) (a) Meyer, B. *Top. Curr. Chem.* **1990**, *154*, 141-208. (b) Paulsen, H. *Angew. Chem.* **1990**, *102*, 851-67. (c) Schmidt, R. R. *Angew. Chem.* **1986**, *25*, 213-236. (d) Kunz, H. *Angew. Chem.* **1987**, *99*, 297-311.

(3) (a) Gabius, H. J. *Angew. Chem.* **1988**, *100*, 1321-1330. (b) Bundle, D. R. 14th International Carbohydrate Symposium (Stockholm/Sweden) 14.8.-19.8.1988.

0002-7863/91/1513-7550$02.50/0

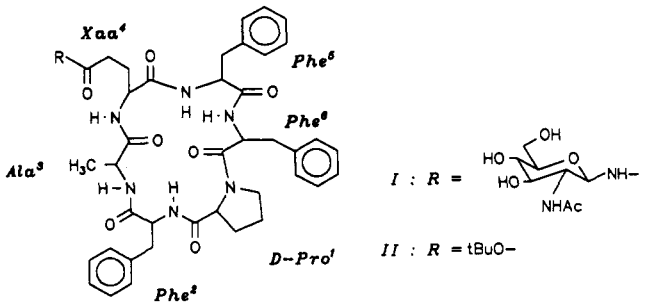

Figure 1. Constitution of glycopeptide I and cyclic hexapeptide II.

oligosaccharide moiety linked to one of the amino acid side chains.[4] Yet conformational analysis is an indispensible tool for understanding the mechanisms of molecular recognition in biological systems.[5] We have therefore focused our attention on the conformations of glycopeptides.

Nuclear magnetic resonance (NMR) spectroscopy is one of the most effective methods for the investigation of the conformation and internal dynamic properties of biomolecules such as peptides,[6] proteins,[6] and glycopeptides.[5a,7] The purpose of this paper is to demonstrate how current 2D NMR spectroscopic techniques and molecular dynamics (MD) simulations in vacuo and in solution lead to a detailed insight into the conformational properties of a synthetic N-glycosylated cyclic hexapeptide, cyclo(-D-Pro[1]-Phe[2]-Ala[3]-[*N*-2-acetamido-2-desoxy-β-D-glucopyranosyl)]-Gln[4]-Phe[5]-Phe[6]) (I), in comparison to the unglycosylated cyclic peptide cyclo(-D-Pro[1]-Phe[2]-Ala[3]-Glu[4](OtBu)-Phe[5]-Phe[6]-) (II). This molecule allowed us to study the influence of a monosaccharide moiety linked to a glutamine side chain on conformation and dynamics of the backbone. A cyclic peptide has been chosen because of the considerable reduction of conformational freedom and flexibility.

There are two main reasons why this particular glycopeptide was chosen for the demonstration of direct glycosylation and conformational analysis.

(i) Model compounds of the type cyclo(-D-Pro[1]-Phe[2]-Ala[3]-Xaa[4]-Phe[5]-Phe[6]-) (where Xaa stands for an amino acid with side chain functionality, e.g., serine or glutamine) have been used in our group to study glycopeptide synthesis by direct glycosylation of larger peptide fragments.[8] It turned out that the partial sequence -Phe-D-Pro-Phe-Ala- generally forms a βII'-turn with D-proline in the $i + 1$ position of these cyclic hexapeptides. It is well known that cyclic hexapeptides have the tendency to form structures containing two β-turns.[9] The strong tendency of a D-Pro residue to adopt the $i + 1$ position of a βII'-turn normally dominates all other effects.[10] Hence, Xaa[4] in our peptides is often in the $i + 1$ position of such a β-turn. The hydroxyl group of a serine[11] or the carboxyl group of a glutamic acid in this position is exposed to the solvent, which provides an ideal opportunity for a glycosylation of their side chain. The synthesis of *O*- and *N*-glycopeptides therefore was a reasonable task.

Scheme I. Synthesis of the Cyclic Hexapeptide II

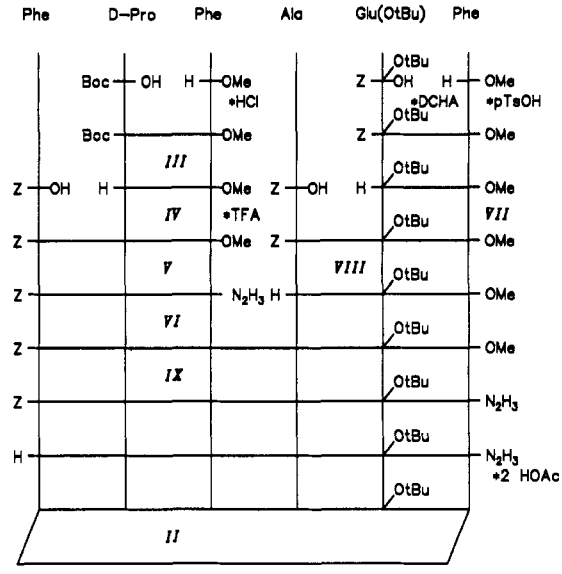

(ii) The model compound cyclo(-D-Pro[1]-Phe[2]-Ala[3]-[*N*-2-acetamido-2-desoxy-β-glucopyranosyl)]Gln[4]-Phe[5]-Phe[6]-] was synthesized as a cyclic retro analogue of the peptide hormone somatostatin and the cyclic decapeptide antamanide. Several cyclopeptides similar in structure have been prepared in our group to study their structure–activity relationship as inhibitor of a hepatocytic transport system.[12] Somatostatin inhibits the secretion of hormones in several tissues such as the hypophysis and pancreas and in the gastrointestinal tract.[13] In addition, it exhibits an anti-ulcerogenic effect[14] and is active as an analgesic.[15] Furthermore, it has been shown that somatostatin can prevent the uptake of various poisons into liver cells.[12d,16] The synthesis of

(4) (a) Ishii, H.; Inoue, Y.; Chujo, R. *Int. J. Pept. Protein Res.* **1984**, *24*, 421–429. (b) Narasinga Rao, B. N.; Bush, C. A. *Biopolymers* **1987**, *26*, 1227–1244. (c) Bush, C. A.; Feeney, R. E. *Int. J. Pept. Protein Res.* **1986**, *28*, 386–397. (d) Gerken, T. A.; Butenhof, K. J.; Shogren, R. *Biochemistry* **1989**, *28*, 5536–5543. (e) Shogren, R.; Gerken, T. A.; Jentoft, N. *Biochemistry* **1989**, *28*, 5525–5536. (f) Taupipat, N.; Mattice, W. L. *Biopolymers* **1990**, *29*, 377–383. (g) Gerken, T. A.; Dearborn, D. G. *Biochemistry* **1984**, *23*, 1485–1497. (h) Gerken, T. A.; Jentoft, N. *Biochemistry* **1987**, *26*, 4689–4699. (i) Gerken, T. A. *Arch. Biochem. Biophys.* **1986**, *247*, 239–253. (j) Mimura, Y.; Inoue, Y.; Joe Maeji, N.; Chujo, R. *Int. J. Pept. Protein Res.* **1989**, *34*, 363–368.

(5) (a) Homans, S. W. *Prog. Nucl. Magn. Reson. Spectrosc.* **1990**, *22*, 55–81. (b) Thiem, J., Ed. *Topics in Current Chemistry*; Springer: Berlin, Heidelberg, New York, 1990; Vol. 154. (c) Atkins, E. D. T., Ed. *Polysaccharides: Topics in Structure and Morphology*; VCH: Weinheim, FRG, 1985.

(6) (a) Kessler, H.; Gehrke, M.; Griesinger, C. *Angew. Chem., Int. Ed. Engl.* **1988**, *27*, 490–536. (b) Ernst, R. R.; Bodenhausen, G.; Wokaun, A. *Principles of Nuclear Magnetic Resonance in One and Two Dimensions*; Clarendon: Oxford. (c) Wüthrich, K. *NMR of Proteins and Nucleic Acids*; John Wiley & Sons: New York, 1986.

(7) Bock, H. *Pure Appl. Chem.* **1983**, *55*, 605–622.

(8) (a) Kling, A. Ph.D. Thesis, Goethe Universität, Frankfurt, FRG, 1989. (b) Kottenhahn, M. Ph.D. Thesis, Goethe Universität, Frankfurt, FRG, 1989. (c) Kottenhahn, M.; Kessler, H. *Liebigs Ann. Chem.* **1991**, 727–744. (d) Kessler, H.; Kottenhahn, M.; Kling, A.; Kolar, C. *Angew. Chem.* **1987**, *99*, 919–921.

(9) Schwyzer, R.; Sieber, P.; Gorup, B. *Chimia* **1958**, *12*, 90–91.

(10) Rose, G. D.; Gierasch, L. M.; Smith, J. A. *Adv. Protein Chem.* **1985**, *37*, 1–109.

(11) Kessler, H.; Kottenhahn, M.; Kling, A.; Matter, H. *Proceedings of the 3rd Akabori Conference*, German-Japanese Symposium on Peptide Chemistry, 2.7.–5.7.1989, Prien/Chiemsee, FRG; Wünsch, E., Ed.; Martinsried, FRG 1989; pp 45–49.

(12) (a) Kessler, H.; Bernd, M.; Damm, I. *Tetrahedron Lett.* **1983**, *23*, 4685–4688. (b) Kessler, H.; Eiermann, V. *Tetrahedron Lett.* **1983**, *23*, 4689–4692. (c) Kessler, H.; Bernd, M.; Kogler, H.; Zarbock, J.; Sørensen, O. W.; Bodenhausen, G.; Ernst, R. R. *J. Am. Chem. Soc.* **1983**, *105*, 6944–6952. (d) Ziegler, K.; Frimmer, M.; Kessler, H.; Damm, I.; Eiermann, V.; Koll, S.; Zarbock, J. *Biochim. Biophys. Acta* **1985**, *845*, 86–93. (e) Kessler, H.; Klein, M.; Müller, A.; Wagner, K.; Bats, J. W.; Ziegler, K.; Frimmer, M. *Angew. Chem., Int. Ed. Engl.* **1986**, *25*, 997–999. (f) Kessler, H.; Gehrke, M.; Haupt, A.; Klein, M.; Müller, A.; Wagner, K. *Klin. Wochenschr.* **1986**, *64*, 74–78. (g) Usadel, K. H.; Kessler, H.; Rohr, G.; Kusterer, K.; Palitzsch, K. D.; Schwedes, U. In *Somatostatin*; Reichlin, S., Ed.; Plenum Publishing Corp.: New York, 1987; pp 193–200. (h) Kessler, H.; Bats, J. W.; Griesinger, C.; Koll, S.; Will, M.; Wagner, K. *J. Am. Chem. Soc.* **1988**, *110*, 1033–1049. (i) Kessler, H.; Gemmecker, G.; Haupt, A.; Klein, M.; Wagner, K.; Will, M. *Tetrahedron* **1988**, *44*, 745–759. (j) Kessler, H.; Klein, M.; Wagner, K. *Int. J. Pept. Protein Res.* **1988**, *31*, 481–498. (k) Kessler, H.; Haupt, A.; Schudok, M.; Ziegler, K.; Frimmer, M. *Int. J. Pept. Prot. Res.* **1988**, *32*, 183–193. (l) Kessler, H.; Gemmecker, G.; Haupt, A.; Lautz, J.; Will, M. *NMR Spectroscopy in Drug Research*; Alfred Benzon Symposium 26; Jaroszewski, J. W., Schaumburg, K., Kofod, H., Eds.; Munksgaard: Copenhagen, Denmark, 1988; pp 138–152. (m) Kessler, H.; Haupt, A.; Will, M. In *Computer-Aided Drug Design*; Perun, T. J., Propst, C. L., Eds.; Marcel Dekker: New York, 1989; pp 461–484. (n) Kessler, H.; Anders, U.; Schudok, M. *J. Am. Chem. Soc.* **1990**, *112*, 5908–5916.

(13) Hotz, J.; Singer, M. V. *Med. Klin. (Munich)* **1982**, *77*, 555–558.

(14) Szabo, S.; Usadel, K. H. *Experientia* **1982**, *38*, 254–255.

(15) Chrubasik, J.; Meynadier, J.; Blond, S.; Scherpereel, P.; Ackermann, E.; Weinstock, M.; Bonath, K.; Cramer, H.; Wünsch, E. *Lancet* **1984**, *24*, 1208–1209.

small cyclic peptides has led to conformationally restricted compounds similar to the compounds discussed here, which show a considerably higher potency with higher selectivity for this process than the native hormone.[12]

Here we report the synthesis and the conformational analysis of the N-glycosylated cyclic hexapeptide cyclo(-D-Pro^1-Phe^2-Ala^3-[*N*-2-acetamido-2-desoxy-β-glucopyranosyl)]Gln^4-Phe^5-Phe^6-) (I) and the cyclic hexapeptide cyclo(-D-Pro^1-Phe^2-Ala^3-Glu(OtBu)^4-Phe^5-Phe^6-) (II) in DMSO-d_6 solution (Figure 1). To our knowledge, it is the first reported conformation of an N-glycosylated cyclic peptide in solution. The structure is used to study the influence of different glycosylated amino acids in the $i + 1$ position of a cyclic hexapeptide β-turn.

Synthesis

The linear precursors of the cyclic hexapeptides were prepared by classical solution-phase methods of peptide synthesis (Scheme I). The coupling of the different precursors was achieved by using the mixed anhydride method with isobutyl chloroformate,[17] the activation of the N-terminal protected compound with EDCI·HCl and HOBt,[18] or the azide-coupling method.[19] After the deprotection of the N-terminal amino acid of the linear hexapeptide, this precursor was cyclisized via the azide by the method of Medzihradsky.[19] Finally the cyclic peptide was purified by semipreparative HPLC and the glutamic acid side chain deprotected with HCl in ether.

N-Glycosylation was achieved by coupling cyclo(-Phe-D-Pro-Phe-Ala-Glu-Phe-) with 2-acetamido-3,4,6-tri-*O*-acetyl-2-desoxy-β-D-glucopyranosylamine according to the classical carbodiimide procedure[18] with EDCI/HOBt in anhydrous THF as solvent. Chromatography of the crude product afforded the *O*-acetyl-protected *N*-glycopeptide with 65% yield in high purity. As with the N-glycosylation of linear peptides,[20] HOBt was added as a scavenger to avoid side reactions from the intermediately formed reactive *O*-acylisourea.

Cleavage of the acetyl protecting groups was carried out with KCN in methanol/ethanol,[21] and subsequent purification by HPLC yielded the deprotected *N*-glycopeptide I (81%). In both reactions, no epimerization at the anomeric carbon atom of the carbohydrate moiety could be observed.

NMR Measurements

Evaluation of the ^{1}H and ^{13}C NMR Spectra of I and II. For the assignment of the ^{1}H resonances, a combination of several 2D NMR techniques was applied for both I and II: In both cases, TOCSY with different mixing times[22] and DQF-COSY[23] provided an almost complete assignment of all proton signals. The amino acid residues of both compounds were identified according to their characteristic pattern of chemical shifts based on connectivity from scalar hetero- and homonuclear couplings. The evaluation of an inverse ^{13}C-^{1}H shift correlation (HMQC[24]) and a HMQC-TOCSY[25] not only confirmed the proton assignments but in addition allowed the complete assignment of all ^{13}C resonances. This made it possible to remove ambiguities in the assignment of the sugar protons. The chemical shifts for the ^{1}H and ^{13}C resonances are given in Table I.

Table I. ^{1}H NMR Chemical Shifts (δ) of I and II in DMSO-d_6 at 300 K[a]

	I (^{1}H)	II (^{1}H)	I (^{13}C)	II (^{13}C)
D-Pro^1-C=O	-	-	171.4	171.4
D-Pro^1-C$_\alpha$H	4.08	4.07	59.7	59.7
D-Pro^1-C$_\beta$H$^{pro\text{-}R}$	1.42	1.42	28.2	28.4
D-Pro^1-C$_\beta$H$^{pro\text{-}S}$	1.63	1.62	-	-
D-Pro^1-C$_\gamma$H$^{pro\text{-}R}$	1.35	1.34	24.4	24.5
D-Pro^1-C$_\gamma$H$^{pro\text{-}S}$	1.79	1.80	-	-
D-Pro^1-C$_\delta$H$^{pro\text{-}R}$	2.70	2.69	46.7	46.8
D-Pro^1-C$_\delta$H$^{pro\text{-}S}$	3.35	3.32	-	-
Phe^2-C=O	-	-	170.6	170.7
Phe^2-NH	8.75 (-6.6)	8.78 (-8.0)	-	-
Phe^2-C$_\alpha$H	4.23	4.22	54.4	54.5
Phe^2-C$_\beta$H$^{pro\text{-}R}$	2.73	2.73	35.8	35.9
Phe^2-C$_\beta$H$^{pro\text{-}S}$	3.26	3.23	-	-
Ala^3-C=O	-	-	172.2	172.4
Ala^3-NH	7.98 (-2.4)	7.99 (-2.6)	-	-
Ala^3-C$_\alpha$H	4.45	4.46	47.2	47.1
Ala^3-C$_\beta$H	1.49	1.52	18.3	18.5
Xaa^4-C=O	-	-	170.1	171.6
Xaa^4-NH	8.12 (-4.0)	8.11 (-4.6)	-	-
Xaa^4-C$_\alpha$H	3.55	3.54	56.0	55.6
Xaa^4-C$_\beta$H^b	1.55	1.50	25.7	25.5
	1.72	1.68	-	-
Xaa^4-C$_\gamma$H^b	1.82	1.77	31.5	30.9
	2.00	1.96	-	-
Xaa^4-OtBu	-	1.38	-	27.8
Xaa^4-N$_\delta$H	7.92 (-5.3)	-	-	-
Phe^5-C=O	-	-	170.7	170.8
Phe^5-NH	7.88 (-2.7)	7.93 (-5.7)	-	-
Phe^5-C$_\alpha$H	4.33	4.37	54.6	54.5
Phe^5-C$_\beta$H$^{pro\text{-}R}$	3.02	3.03	36.4	36.5
Phe^5-C$_\beta$H$^{pro\text{-}S}$	3.18	3.21	-	-
Phe^6-C=O	-	-	168.5	168.4
Phe^6-NH	7.28 (-0.9)	7.28 (+0.4)	-	-
Phe^{6}C$_\alpha$H	4.64	4.65	53.1	53.2
Phe^{6}C$_\beta$H$^{pro\text{-}S}$	2.79	2.78	38.8	38.5
Phe^{6}C$_\beta$H$^{pro\text{-}R}$	3.09	3.08	-	-
GlcNAc-C$_{(1)}$H	4.81	-	79.0	-
GlcNAc-C$_{(2)}$H	3.52	-	54.6	-
GlcNAc-C$_{(3)}$H	3.36	-	74.5	-
GlcNAc-C$_{(4)}$H	3.10	-	78.7	-
GlcNAc-C$_{(5)}$H	3.11	-	70.5	-
GlcNAc-C$_{(6)}$H^b	3.44	-	60.9	-
	3.66	-	-	-
GlcNAc-N$_{(2)}$H	7.86 (-4.3)	-	-	-
GlcNAc-O$_{(3)}$H	*c*	-	-	-
GlcNAc-O$_{(4)}$H	4.99	-	-	-
GlcNAc-O$_{(6)}$H	*c*	-	-	-

[a] All data are given in parts per million. Temperature gradients of N*H* protons (ppb/K) are given in parentheses. [b] No diastereotopic assignment. [c] Value could not be obtained.

Sequential assignment of the amino acid residues was carried out from the analysis of ROESY[26] and NOESY[27] spectra with mixing times of 120 ms. The obtained information was cross-checked and verified in a selective inverse ^{13}C-^{1}H long-range correlation applied to the carbonyl carbons (HMBC[28,29]). As we recently reported, the quality of this correlation for the sequencing and assignment of carbonyl resonances could be improved by using a 270° Gaussian-shaped pulse[29c] for the semisoft exci-

(16) Usadel, K. H.; Kessler, H.; Rohr, G.; Kusterer, K.; Palitzsch, K. D.; Schwedes, U. *Klin. Wochenschr.* **1986**, *64*, 59-63.
(17) Vaughn, J. R.; Osato, R. L. *J. Am. Chem. Soc.* **1952**, *74*, 676-678.
(18) Sheehan, J. C.; Cruickshank, P. A. *J. Org. Chem.* **1961**, *26*, 2525-2528.
(19) Klausner, Y. S.; Bodanszky, M. *Synthesis* **1974**, 549-559.
(20) Bodanszky, M. *Principles of Peptide Synthesis*; Springer: Berlin, FRG, 1984.
(21) Herzig, J.; Nudelman, A.; Gottlieb, H. E.; Fischer, B. *J. Org. Chem.* **1986**, *51*, 727-730.
(22) (a) Braunschweiler, L.; Ernst, R. R. *J. Magn. Reson.* **1983**, *53*, 521-528. (b) Bax, A.; Byrd, R. A.; Aszalos, A. *J. Am. Chem. Soc.* **1984**, *106*, 7632-7633. (c) Bax, A.; Davis, D. G. *J. Magn. Reson.* **1985**, *65*, 355-360.
(23) (a) Piantini, U.; Sørensen, O. W.; Ernst, R. R. *J. Am. Chem. Soc.* **1982**, *104*, 6800-6801. (b) Rance, M.; Sørensen, O. W.; Bodenhausen, G.; Wagner, G.; Ernst, R. R.; Wüthrich, K. *Biochem. Biophys. Res. Commun.* **1983**, *117*, 458-479.
(24) (a) Müller, L. *J. Am. Chem. Soc.* **1979**, *101*, 4481-4484. (b) Bax, A.; Griffey, R. H.; Hawkins, L. B. *J. Magn. Reson.* **1983**, *55*, 301-315.
(25) (a) Lerner, A.; Bax, A. *J. Magn. Reson.* **1986**, *69*, 375-380. (b) Kessler, H.; Bermel, W.; Griesinger, C. Presented at the Sixth Meeting of the Fachgruppe Magnetische Resonanzspektroskopie, Berlin, September 25-28, 1985.
(26) (a) Bothner-By, A. A.; Stephens, R. L.; Lee, J.; Warren, C. D.; Jeanloz, R. W. *J. Am. Chem. Soc.* **1984**, *106*, 811-813. (b) Bax, A.; Davis, D. G. *J. Magn. Reson.* **1985**, *63*, 207-213. (c) Kessler, H.; Griesinger, C.; Kerssebaum, R.; Wagner, K.; Ernst, R. R. *J. Am. Chem. Soc.* **1987**, *109*, 607-609.
(27) Jeener, J.; Meier, B. H.; Bachmann, P.; Ernst, R. R. *J. Chem. Phys.* **1979**, *71*, 4546-4553.
(28) Bax, A.; Summers, M. F. *J. Am. Chem. Soc.* **1986**, *108*, 2093-2094.
(29) (a) Bermel, W.; Wagner, K.; Griesinger, C. *J. Magn. Reson.* **1989**, *83*, 223-232. (b) Emsley, L.; Bodenhausen, G. *J. Magn. Reson.* **1989**, *82*, 211-221. (c) Kessler, H.; Schmieder, P.; Köck, M.; Kurz, M. *J. Magn. Reson.* **1990**, *88*, 615-618.

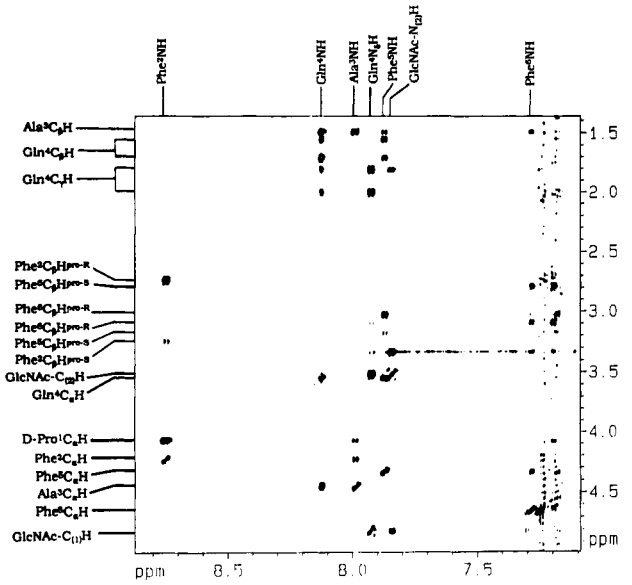

Figure 2. N*H*/C$_\alpha$H region of the 600-MHz NOESY spectrum (120-ms mixing time) of the glycopeptide I in DMSO-d_6. Only positive contours are shown. Zero quantum contributions are not suppressed, as integration of zero quantum contribution is zero. These signals are easy to recognize by their antiphase appearance.

tation of the C=O resonances because this self-refocusing pulse allows a phase-sensitive recording in F_1. This experiment is not only important for the assignment of the C=O resonances but can also be applied for a diastereotopic assignment of C$_\beta$*H* resonances.

Extraction of Conformationally Relevant NMR Parameters. Only one distinct set of signals was found in the ^{1}H and ^{13}C NMR spectra of II. A second signal set with a population <1% could be detected in the ^{1}H NMR spectrum of I, but a detailed examination of this conformation was impossible due to the low signal to noise ratio. It is not clear if this second set of signals is an indication of a second conformation (lack of 2D ROESY exchange peaks) or an impurity (no indication in HPLC analysis). No conformational change slow on the NMR time scale could be determined by line-broadening effects. All other criteria for conformational homogeneity were fulfilled.[30] However, these observations cannot exclude the occurrence of fast interconverting conformers. It is known that various side chains of amino acids in smaller peptides or cyclopeptides and exocyclic (e.g., glycosidic) bonds of saccharide moieties are not rigid or fixed in one distinct conformation. Often a conformational equilibrium has to be postulated in peptidic backbones as well, where fast dynamical interconversions have been observed.[31,32] Conformational analysis by NMR spectroscopy on several cyclic pentapeptides as models for reverse turns reveals that two different turn structures (βI- and βII-turn) are present in equilibrium.[31e]

In fact, it is difficult to decide whether a molecule is conformationally homogeneous or not. However, at the end of the conformational analysis, the results are checked for the validity of the assumption of one dominating conformer. If all NMR data agree with a unique conformation, then this approach is a sufficient model.[31a,b] However, as will be pointed out later, this was not the case here.

Conformational analysis is based on distances between protons derived from proton–proton dipolar interactions. NOESY and ROESY experiments at 600 MHz with mixing times of 120 ms provide quantitative information on interproton distances. They were recorded without zero-quantum suppression. Most of the peak volumes were integrated on both sides of the diagonal; some cross peak intensities could not be determined, mainly due to t_1 noise. The distances were calculated under the assumption of an isotropic tumbling rigid molecule and by using the isolated two-spin approximation (ISPA). The volume of the cross peak between spins i and j then is proportional to d_{ij}^{-6}.[33]

For assignment of NOE effects from overlapping proton resonances in the N-glycosylated cyclic hexapeptide, HMQC-NOESY first described by Shon and Opella for ^{15}N-labeled proteins[34] was applied. The ^{1}H homonuclear NOE between overlapping proton resonances could be detected with ^{1}H/^{13}C heteronuclear correlated spectroscopy in natural ^{13}C abundance. This experiment provides the means of establishing proton-homonuclear NOE's resolved by a heteronuclear shift correlation. BIRD presaturation of the ^{12}CH protons and ^{13}C GARP decoupling during the detection period was applied. The application of the HMQC-NOESY to peptides in natural abundance at higher concentration even allows a quantification of the NOE effects.[35]

For the glycopeptide I, we obtained an NOE data set consisting of 57 proton–proton distances (including all NOE's to diastereotopically assigned protons, see Table IV). For calibration of the NOESY integrals, the cross peak between Phe^{6}C$_\beta$*H*$^{pro-R}$ and Phe^{6}C$_\beta$*H*$^{pro-S}$ was used. The resulting N*H*–N*H* distances in comparison with data derived from the ROESY (Table IV, values in parentheses, both were measured at 600 MHz) exhibit the contribution of chemical exchange to the volume integral of the NOESY/ROESY cross peaks.[6c,33] Chemical exchange increases the value for the NOESY cross peak integral (shortening the derived distance), but decreases the integral value in the measured ROESY spectra—because of the different sign of the NOE/ROE effects for molecules of this size (positive and negative cross peak amplitudes in 600-MHz spectra). Therefore, the NOESY-derived N*H*–N*H* distances were taken as the lower bounds and the ROESY-derived distances as the upper bounds in the distance constraints term for the refinement procedure described below. However, it was not possible to separate quantitively the contribution of the chemical exchange from the contribution of the dipolar relaxation to get more reliable distances. The experimental error for all other NOE-derived distances was estimated as 5–10%, when distances obtained from NOESY and ROESY experiments were compared.

For II, we obtained 30 distances (including all NOE's to diastereotopically assigned protons) from the 2D NOESY spectrum (Table V). The comparison of observed and calculated distances (40-ps MD trajectory) shows a systematic deviation, also indicated by a high value for the average restrained violation, caused by an incorrect calibration due to experimental inaccuracies. Better agreement between experiment and simulation was observed by shortening all experimental distances by about 5%. We have used the internal consistence of the data set as criterion for an iterative recalibration without employing a precise calibration cross peak.

In addition to NOE's, scalar coupling constants of vicinal nuclei provide conformational information of the involved dihedral angles via the Karplus equations[30c,36] (Table II). The N*H*–C$_\alpha$*H* coupling constants were extracted from 1D spectra after resolution enhancement.

(30) (a) Kessler, H.; Bermel, W.; Müller, A.; Pook, K. H. In *The Peptides, Analysis, Synthesis, Biology*; Udenfriend, S., Meienhofer, J., Hruby, V. R., Eds.; Verlag Chemie: Weinheim, 1986; Vol. 7, pp 437–472. (b) Kessler, H.; Bermel, W. In *Methods in Stereochemical Analysis*; Croasmun, W. R., Marchand, P., Eds.; VCH: Deerfield Beach, FL, 1987; Vol. 9, pp 259–299. (c) Kessler, H. *Angew. Chem., Int. Ed. Engl.* **1982**, *21*, 512–523.

(31) (a) Kessler, H.; Bats, J. W.; Lautz, J.; Müller, A. *Liebigs Ann. Chem.* **1989**, 913–928. (b) Kessler, H.; Griesinger, C.; Lautz, J.; Müller, A.; van Gunsteren, W. F.; Berendsen, H. J. C. *J. Am. Chem. Soc.* **1988**, *110*, 3393–3396. (c) Kopple, K. D.; Bhandary, K. K.; Kartha, G.; Wang, Y. S.; Parameswaran, K. N. *J. Am. Chem. Soc.* **1986**, *108*, 4637–4642. (d) Kopple, K. S.; Wang, Y. S.; Cheng, A. G.; Bhandary, K. K. *J. Am. Chem. Soc.* **1988**, *110*, 4168–4176. (e) Stradley, S. J.; Rizo, J.; Bruch, M. D.; Stroup, A. N.; Gierasch, L. M. *Biopolymers* **1990**, *29*, 263–287.

(32) Rowan, R.; Warshel, A.; Sykes, B. D.; Karplus, M. J. *Biochemistry* **1974**, *13*, 970.

(33) Neuhaus, D.; Williamson, M. *The Nuclear Overhauser Effect in Structural and Conformational Analysis*; VCH: Weinheim, FRG, 1989.

(34) (a) Shon, K.; Opella, S. J. *J. Magn. Reson.* **1989**, *82*, 193–197. (b) Crouch, R. C.; Andrews, C. W.; Martin, G. E.; Luo, J. K.; Castle, R. N. *Magn. Reson. Chem.* **1990**, *28*, 774–778.

(35) Kessler, H.; Gemmecker, G.; Matter, H. Unpublished results.

(36) (a) Karplus, M. J. *J. Chem. Phys.* **1959**, *30*, 11–15. (b) Bystrov, V. F. *Prog. Nucl. Magn. Reson. Spectrosc.* **1976**, *10*, 41–81.

Table II. Comparison of Experimentally Determined and Calculated $^3J(NH,C_\alpha H)$ Coupling Constants (Hz) for I and II[a]

Compound I

	Phe^2	Ala^3	Gln^4	Gln$N_\delta H^4$	Phe^5	Phe^6	GlcNAc
$^3J_{NH,\alpha}$	9.0	9.2	4.0	8.8	8.1	6.6	8.6
φ_{expt}	−139.3	−137.2	−173.6	−141.2	*−147.1*	*−157.5*	−143.0
	−100.7	*−102.8*	*−66.6*	*−98.8*	−92.9	−82.5	−97.0
	−	−	104.7	−	−	84.4	−
	−	−	15.3	−	−	35.6	−
$\langle^3J_{calcd}\rangle^a$	7.8	9.9	5.0	10.1	6.6	11.8	11.2
$\langle^3J_{calcd}\rangle^b$	6.8	10.9	3.2	9.8	7.1	8.3	10.7
$\langle^3J_{calcd}\rangle^{av}$	7.3	10.4	4.1	9.9	6.8	10.0	10.9
$\langle^3J_{calcd}\rangle^c$	8.4	9.2	6.2	10.3	8.2	8.3	9.5

Compound II

	Phe^2	Ala^3	Glu^4	Phe^5	Phe^6
$^3J_{NH,\alpha}$	9.0	8.8	3.9	9.1	6.8
φ_{expt}	−139.3	−141.2	−174.3	*−138.3*	*−160.0*
	−100.7	*−98.8*	*−65.7*	−101.7	−40.0
	−	−	105.5	−	133.1
	−	−	14.5	−	−13.1
$\langle^3J_{calcd}\rangle^a$	8.1	9.7	3.9	8.2	11.6
$\langle^3J_{calcd}\rangle^b$	6.4	10.6	5.4	8.2	10.5
$\langle^3J_{calcd}\rangle^{av}$	7.3	10.1	4.6	8.2	11.1

[a] Possible values for the corresponding peptide backbone angles φ (deg) are given, obtained from Bystrovs KARPLUS equation. The experimental values are determined from the 1D spectrum after resolution enhancement; the calculated values $\langle^3J_{calcd}\rangle$ are obtained by averaging over MD simulations. The superscript indicates the numbering of the simulation. Compound I: a, MDI^a; b, MDI^b; c, MDI^c (with time-dependent distance constraints). Compound II: a, MDII^a; b, MDII^b. $\langle^3J_{calcd}\rangle^{av}$ indicates the values obtained from averaging over two different simulations, as described in text.

Finally the temperature dependencies of amide proton chemical shifts indicate their inclusion in inter- or intramolecular hydrogen bonds (Table I).[30c] As indicated, the large temperature gradients of the NH protons Phe^{2}N$^\alpha$H, Gln^{4}N$^\alpha$H, Gln^{4}N$^\delta$H, and GlcN^{2}H are oriented externally. Small coefficients (internal orientation) are found for Phe^{6}N$^\alpha$H and Ala^{3}N$^\alpha$H. The coefficient for Phe^{5}N$^\alpha$H is in intermediate range.

Conformation of the Side Chains. The populations of different side chain rotamers were determined via coupling constants following standard procedures.[37] The $C_\beta H$–$C_\alpha H$ coupling constants for diastereotropic C_β protons were extracted from E.COSY spectra[38] in both cases. For glutamine or glutamic acid, it was not possible to derive these coupling constants due to signal overlap and spin systems with more than three coupled protons.

The diastereotopic assignment of C_β protons was achieved via the inverse COLOC experiment with semisoft excitation of the carbonyls with a Gaussian-shaped 270° pulse (HMBCS-270°).[29c] Extraction of heteronuclear long-range coupling constants is not as easy as in the case of a normal COLOC experiment.[37] In the latter, the transfer amplitude I_{ij} from proton i to carbon j is modulated by $\sin^2$ of the heteronuclear coupling $J(H^i,C_j)$, but in the nonrefocused HMBC spectra is modulated only by sin of this coupling. Therefore antiperiplanar and synclinal couplings are better discriminated in the H,C-COLOC spectrum than in HMBC. However, with known $C_\alpha H$–$C_\beta H$ coupling constants, a calculation of peak intensities yields a reliable discrimination also for HMBC.[39]

The values for the $C_\beta H$–$C_\alpha H$ coupling constants and the derived side chain conformations under the assumption of staggered conformations[40] are summarized in Table III.

From the interpretation of NOE effects, no ambiguities were found for diastereotopic assignment.[41] Another argument for the described side chain preference for Phe^6 is that the preferred position of the aromatic ring over the pyrrolidine ring system of D-proline causes a large splitting of the two D-Pro^1-$C_\delta H$ chemical shifts (δ) due to anisotropy effects.[12h]

Table III. $^3J(C_\alpha H,C_\beta H)$ Coupling Constants (Hz) and Calculated Populations for the Side Chain Conformers for I and II[a]

Compound I

residue	Phe^2	Phe^5	Phe^6
$^3J(C_\alpha H,C_\beta H^{pro\text{-}R})$	11.7	10.6	4.6
$^3J(C_\alpha H,C_\beta H^{pro\text{-}S})$	3.2	4.1	9.2
$\chi_1 = -60°$	83%	73%	18%
$\chi_1 = 180°$	5%	14%	60%
$\chi_1 = 60°$	12%	14%	22%

Compound II

residue	Phe^2	Phe^5	Phe^6
$^3J(C_\alpha H,C_\beta H^{pro\text{-}R})$	11.5	11.7	4.3
$^3J(C_\alpha H,C_\beta H^{pro\text{-}S})$	3.8	3.4	9.1
$\chi_1 = -60°$	83%	77%	17%
$\chi_1 = 180°$	7%	11%	59%
$\chi_1 = 60°$	10%	12%	24%

[a] The values are obtained from 250-MHz E.COSY spectrum; the populations are calculated by using Pachler's equation. The diastereotopic assignment of β-protons was achieved via heteronuclear coupling constants and interpretation of NOE data.

Conformational Analysis of I and II. Under the incorporation of some characteristic backbone NOE's, a crude model structure could be built on the basis of the experimental derived Phe^{6}NH—Ala^{3}C=O and Ala^{3}NH—Phe^{6}C=O hydrogen-binding pattern, forming a βII′/βII-type structure. Two small NOE's between Gln$^4C_\alpha H$–Phe^{5}NH and Phe$^5C_\alpha H$–Phe^{5}NH lead to the assumption of a βII-turn in this region. The "ideal" values for these $C_\alpha H^{i-1}$–NH^i and $C_\alpha H^i$–NH^i NOE's in a βII-turn are 205–220 pm. The observed values here (231 and 244 pm, respectively) correspond well to these data.

NOE's in agreement with an assumed additional conformation with βI-turn are Phe^{5}NH–Ala$^3C_\beta H$ and Phe^{5}NH–Phe$^5C_\beta H^{pro\text{-}S}$. These NOE's are only possible in βI-turn geometry. The homonuclear coupling constants are in agreement with both types of turn structures, so that discrimination at this stage cannot be carried out. The weak HMBC cross peak observed between Glu^{4}C=O and Phe$^5C_\alpha H$ is in agreement with the βII-turn; this ^3J(C,H) coupling is only observable when the involved nuclei adopt an antiperiplanar orientation.

In the other moiety of the peptide, the postulated βII′-turn structure is supported by the characteristic NOE's and homonuclear J coupling constants for this type of structure.

Structure Refinement by Molecular Dynamics Simulation (MD)

In order to translate the proton–proton distances and other experimental parameters into a three-dimensional molecular structure, restrained and unrestrained molecular dynamics (MD) simulations using the GROMOS program library[42] was utilized. For generation of the coordinates of the starting structures and interactive modeling, the program INSIGHT (BIOSYM) was used. The starting coordinates for the glycopeptide I were taken from a recently obtained structure of the similar cyclic hexapeptide cyclo(−D-Pro^1–Phe^2–Ala^3–Ser^4–Phe^5–Phe^6–);[11] the carbohydrate part was connected to the glutamine side chain by computer model building. As starting coordinates for the cyclic hexapeptide II,

(37) (a) Kessler, H.; Griesinger, C.; Wagner, K. *J. Am. Chem. Soc.* **1987**, *109*, 6927–6933. (b) Anders, U.; Gemmecker, G.; Kessler, H.; Griesinger, C. *Fresenius' Z. Anal. Chem.* **1987**, *327*, 72–73.

(38) (a) Griesinger, C.; Sørensen, O. W.; Ernst, R. R. *J. Am. Chem. Soc.* **1985**, *107*, 6394–6396. (b) Griesinger, C.; Sørensen, O. W.; Ernst, R. R. *J. Chem. Phys.* **1986**, *85*, 6837–6852.

(39) Hofmann, M.; Gehrke, M.; Bermel, W.; Kessler, H. *Magn. Reson. Chem.* **1989**, *27*, 877–886.

(40) (a) Pachler, K. G. R. *Spectrochim. Acta* **1963**, *19*, 2085–2092. (b) Pachler, K. G. R. *Spectrochim. Acta* **1964**, *20*, 581–587.

(41) Wagner, G.; Braun, W.; Havel, T. F.; Schaumann, T.; Go, N.; Wüthrich, K. *J. Mol. Biol.* **1987**, *196*, 611–639.

(42) (a) Aquist, J.; van Gunsteren, W. F.; Leijonmark, M.; Tupia, O. J. *J. Mol. Biol.* **1985**, *183*, 461–477. (b) van Gunsteren, W. F.; Kaptein, R.; Zuiderweg, E. R. P. *Proceedings of the NATO/CECAM Workshop on Nucleic Acid Conformation and Dynamics*; Olsen, W. K., Ed.; Orsay, 1983; pp 79–92. (c) van Gunsteren, W. F.; Boelens, R.; Kaptein, R.; Scheek, R. M.; Zuiderweg, E. R. P. In *Molecular Dynamics and Protein Structure*; Hermans, J., Ed.; Polycrystal Book Service: Western Springs, IL, 1985; pp 92–99. (d) Biomos, B. V.: Nijenborgh 16 NL 9747 AG Groeningen, Groeningen; Molecular Simulation (GROMOS) Library Manual; van Gunsteren, W. F.; Berendsen, H. J. C. *GROMOS user manual*; pp 1–229.

Table IV. Comparison of Experimental and Calculated Proton–Proton Distances (pm) for the Glycopeptide I[a]

protons		NOESY	MDI[a]	MDI[b]	MDI_{av}	MDI[c]
Ala^3NH	Phe^2NH	227 (319)	255	260	258	276
Phe^5NH	Gln^4NH	282 (382)	416	302	359	375
Phe^5NH	Phe^6NH	228 (305)	285	276	280	286
Phe^5NH	$Phe^5C_\alpha H$	244[d]	213	270	242	252
Phe^5NH	$Gln^4C_\alpha H$	231[d]	193	344	269	272
Phe^5NH	$Ala^3C_\beta H$	322[b]	565	389	477	483
Phe^5NH	$Phe^5C_\beta H^{pro\text{-}R}$	267	367	245	306	293
Phe^5NH	$Phe^5C_\beta H^{pro\text{-}S}$	338	408	350	379	374
Phe^5NH	$Gln^4C_\beta H$	283[c]	398	323	361	378
Phe^5NH	$Gln^4C_\gamma H$	407	435	460	448	468
$Phe^5C_\alpha H$	$Phe^5C_\beta H^{pro\text{-}S}$	244	241	245	243	242
$Phe^5C_\alpha H$	$Phe^5C_\beta H^{pro\text{-}R}$	283	286	290	288	287
Phe^6NH	$Phe^6C_\alpha H$	258	285	273	279	268
Phe^6NH	$Phe^5C_\alpha H$	312	340	338	339	315
Phe^6NH	$Phe^6C_\beta H^{pro\text{-}S}$	295	266	304	285	293
Phe^6NH	$Phe^6C_\beta H^{pro\text{-}R}$	308	313	344	329	323
Phe^6NH	$Phe^5C_\beta H^{pro\text{-}R}$	347	324	324	324	351
Phe^6NH	$Phe^5C_\beta H^{pro\text{-}S}$	359	397	400	398	398
Phe^6NH	$Ala^3C_\beta H$	321[b]	401	374	388	451
Phe^6NH	$D\text{-}Pro^1C_\delta H$	378[c]	429	407	418	413
Phe^6NH	$Gln^4C_\alpha H$	377	381	411	396	393
$Phe^6C_\alpha H$	$Phe^6C_\beta H^{pro\text{-}R}$	247	236	238	237	235
$Phe^6C_\alpha H$	$Phe^6C_\beta H^{pro\text{-}S}$	276	288	289	289	288
$Phe^6C_\alpha H$	$D\text{-}Pro^1C_\delta H$	215[c]	218	218	218	223
$D\text{-}Pro^1C_\alpha H$	$D\text{-}Pro^1C_\delta H$	225[c]	244	245	244	241
$D\text{-}Pro^1C_\alpha H$	Ala^5NH	307	352	359	355	364
Phe^2NH	$Phe^2C_\beta H^{pro\text{-}S}$	238	240	240	240	243
Phe^2NH	$Phe^2C_\beta H^{pro\text{-}R}$	324	348	347	347	351
Phe^2NH	$Phe^2C_\alpha H$	280	276	274	275	276
Phe^2NH	$Ala^3C_\beta H$	380[b]	504	517	510	505
Phe^2NH	$D\text{-}Pro^1C_\alpha H$	203	209	207	208	211
Phe^2NH	$D\text{-}Pro^1C_\beta H$	352[c]	382	387	384	376
$Phe^2C_\alpha H$	$Phe^2C_\beta H^{pro\text{-}R}$	300	289	290	289	289
$Phe^2C_\alpha H$	$Phe^2C_\beta H^{pro\text{-}S}$	261	243	243	243	242
Ala^3NH	$Phe^2C_\alpha H$	288	329	330	329	307
Ala^3NH	$Ala^3C_\alpha H$	266	284	286	285	280
Ala^3NH	$Phe^2C_\beta H^{pro\text{-}S}$	354	406	402	404	408
Ala^3NH	$Phe^2C_\beta H^{pro\text{-}R}$	362	331	325	328	355
Ala^3NH	$Ala^3C_\beta H$	246[b]	280	283	281	293
$Ala^3C_\alpha H$	$Ala^3C_\beta H$	240[b]	242	241	241	241
Gln^4NH	$Ala^3C_\alpha H$	235	243	238	240	245
Gln^4NH	$Gln^4C_\alpha H$	260	270	265	267	267
Gln^4NH	$Gln^4C_\beta H$	234[c]	255	225	240	259
Gln^4NH	$Ala^3C_\beta H$	235[b]	338	344	341	346
Gln^4NH	$Gln^4C_\gamma H$	290[c]	385	424	405	395
$Gln^4C_\alpha H$	$Gln^4C_\beta H$	253[c]	259	252	256	253
$Gln^4C_\alpha H$	$Gln^4C_\gamma H$	266[c]	285	301	293	310
$Gln^4N_\delta H$	$Gln^4C_\beta H$	376[c]	434	438	436	394
$Gln^4N_\delta H$	$Gln^4C_\gamma H$	237[c]	258	253	256	273
$Gln^4N_\delta H$	$GlcNAc\text{-}H^1$	288	283	283	283	283
$Gln^4N_\delta H$	$GlcNAc\text{-}H^2$	229	251	249	250	266
$Gln^4N_\delta H$	$GlcNAc\text{-}H^5$	359	444	446	445	428
$GlcNAcN^2H$	$GlcNAc\text{-}H^1$	288	265	262	264	283
$GlcNAcN^2H$	$Gln^4C_\gamma H$	247[c]	473	470	471	426
$GlcNAcN^2H$	$GlcNAc\text{-}H^2$	229	279	277	278	258
$GlcNAc\text{-}H^1$	$Phe^5C_\alpha H$	327	354	334	344	442
$GlcNAc\text{-}H^1$	$GlcNAc\text{-}H^2$	297	292	292	292	292

[a] For the notation of the different MD trajectories, please see text. The distance data given in parentheses are values obtained from a 600-MHz ROESY spectrum; they are also included in the distance constraints data file. [b] Increased by 100 pm for MD run (CH_3 group (ref 42b)). [c] Increased by 90 pm for MD run (CH_2 without diastereotopic assignment (ref 42b)). [d] NOE's omitted in the MD run MDI[b] (see text).

the coordinates of the determined averaged solution structure of I with the exception of the saccharide moiety was used. The starting structure was built according to the NMR-derived hydrogen bond patterns in both cases; some NMR derived distances have also been included in this manual model-building procedure. All peptide bonds were assumed to be in the trans configuration ($\omega = 180°$), because there was no experimental indication (^{13}C chemical shift of D-Pro-C_β, D-Pro-C_γ resonances, NOE data) for a cis orientation.[12n,30c,43,44,45] The side chains for I and II were

Table V. Comparison of Experimental and Calculated Proton–Proton Distances (pm) for the Cyclic Hexapeptide II[a]

protons		NOESY	MDII[a]	MDII[b]	$MDII_{av}$
Phe^5NH	$Phe^5C_\alpha H$	240[d]	207	274	240
Phe^5NH	$Glu^4C_\alpha H$	239[d]	200	344	269
Phe^5NH	$Phe^5C_\beta H^{pro\text{-}R}$	261	358	251	304
Phe^5NH	$Phe^5C_\beta H^{pro\text{-}S}$	397	373	355	377
Phe^5NH	$Glu^4C_\beta H$	342[d]	382	356	369
Phe^6NH	$Phe^6C_\alpha H$	291	285	282	283
Phe^6NH	$Phe^5C_\alpha H$	323	337	339	336
Phe^6NH	$Phe^6C_\beta H^{pro\text{-}R}$	300	274	324	319
Phe^6NH	$Phe^6C_\beta H^{pro\text{-}S}$	316	266	279	273
$Ph3^6NH$	$Ala^3C_\beta H$	334[b]	440	421	431
$Phe^6C_\alpha H$	$Phe^6C_\beta H^{pro\text{-}R}$	254	250	235	235
$Phe^6C_\alpha H$	$D\text{-}Pro^1C_\delta H$	223[c]	217	220	219
$D\text{-}Pro^1C_\alpha H$	$D\text{-}Pro^1C_\beta H$	238[c]	241	244	243
$D\text{-}Pro^1C_\alpha H$	Ala^5NH	334	359	374	369
Phe^2NH	$Phe^2C_\beta H^{pro\text{-}R}$	236	244	245	244
Phe^2NH	$Phe^2C_\beta H^{pro\text{-}S}$	386	352	349	350
Phe^2NH	$Phe^2C_\alpha H$	292	278	272	274
Phe^2NH	$D\text{-}Pro^1C_\alpha H$	200	208	206	206
Phe^2NH	$D\text{-}Pro^1C_\beta H$	407[c]	386	389	387
Ala^3NH	$Phe^2C_\alpha H$	303	324	337	335
Ala^3NH	$Ala^3C_\alpha H$	303	285	286	285
Ala^3NH	$Phe^2C_\beta H^{pro\text{-}S}$	363	367	386	389
Ala^3NH	$Ala^3C_\beta H$	242[b]	286	287	283
$Ala^3C_\alpha H$	$Ala^3C_\beta H$	233[b]	241	239	240
Glu^4NH	$Ala^3C_\alpha H$	229	243	226	234
Glu^4NH	$Glu^4C_\alpha H$	267	266	236	251
Glu^4NH	$Glu^4C_\beta H$	235[c]	273	299	286
Glu^4NH	$Glu^4C_\chi H$	336[c]	328	350	340
$Glu^4C_\alpha H$	$Glu^4C_\beta H$	267[c]	258	224	241
$Glu^4C_\alpha H$	$Glu^4C_\chi H$	349[c]	309	372	339

[a] For the notation of the different MD trajectories, please see text. [b] Increased by 100 pm for MD run (CH_3 group (ref 42b)). [c] Increased by 90 pm for MD run (CH_2 without diastereotopic assignment (ref 42b)). [d] NOE's omitted in the MD run MDII[b] (see text).

fixed in their dominantly populated conformer (Table III).[12c]

The GROMOS force field contains parameters for simulations of peptide/protein and nucleic acid structures. Different parameters for this force field are available for calculations under different conditions: in vacuo,[42b] in an aqueous environment,[42] and in an apolar environment.[46] Earlier MD simulations of different cyclodextrines (a family of cyclic oligosaccharides consisting of six, seven, or eight glucose units) suggest that the GROMOS force field is reliable for MD simulations of oligosaccharides or glycopeptides.[47] Including the *N*-2-acetamido-2-desoxy-β-glucopyranosyl) residue (GlcNAc) in the MD simulations, some new parameters have to be incorporated in the employed force field. These values for the monosaccharide residue are derived from parameters listed in ref 47a.

The kinetic energy was included during the calculations by coupling the whole system to a thermal bath.[48] All calculations were performed on Silicon Graphics 4D/240SX and 4D/70GTB computers.

The temperature gradients of the chemical shifts of the N*H* resonances (Table I) were implemented as described before[12h] as factors for reducing the charges of the solvent exposed amide protons and nitrogens: Full charge was left at the observed temperature gradient of −0.9 ppb/K for Phe^6NH, whereas for Phe^1NH ($\Delta\delta/\Delta t = -6.6$ ppb/K), a reduction to 25% was used in the case of I. Intermediate values were linearly interpolated.

(43) (a) Mierke, D. F.; Yamazaki, T.; Said-Nejad, O. E.; Felder, E. R.; Goodman, M. *J. Am. Chem. Soc.* **1989**, *111*, 6847–6849. (b) Bairaktari, E.; Mierke, D. F.; Mammi, S.; Peggion, E. *J. Am. Chem. Soc.* **1990**, *112*, 5383.
(44) Deber, C. M.; Madison, V.; Blout, E. R. *Acc. Chem. Res.* **1976**, *9*, 106.
(45) Siemion, I. Z.; Wieland, T.; Pook, K. H. *Angew. Chem., Int. Ed. Engl.* **1975**, *14*, 702.
(46) Lautz, J.; Kessler, H.; Kaptein, R.; van Gunsteren, W. F. *J. Comput.-Aided Mol. Des.* **1987**, *1*, 219–241.
(47) (a) Köhler, J. E. H.; Saenger, W.; van Gunsteren, W. F. *Eur. Biophys. J.* **1987**, *15*, 197–210. (b) Köhler, J. E. H.; Saenger, W.; van Gunsteren, W. F. *Eur. Biophys. J.* **1987**, *15*, 211–224. (c) Köhler, J. E. H.; Saenger, W.; van Gunsteren, W. F. *Eur. Biophys. J.* **1988**, *16*, 153–168. (d) Köhler, J. E. H.; Saenger, W.; van Gunsteren, W. F. *J. Mol. Biol.* **1988**, *203*, 241–250. (e) Köhler, J. E. H.; Saenger, W.; van Gunsteren, W. F. *J. Biomol. Struct. Dyn.* **1988**, *6*, 181–198.
(48) Berendsen, H. J. C.; Postma, J. P. M.; van Gunsteren, W. F.; Di Nola, A.; Haak, J. R. *J. Chem. Phys.* **1984**, *81*, 3684–3690.

The temperature gradients for the amide protons of the saccharide moiety show that these protons are exposed to the solvent; charge reduction in this case is applied. The same concept was used during the simulation of II. A full effective charge was left for Phe^{6}NH ($\Delta\delta/\Delta t$ = +0.4 ppb/K); the charge values for Phe^{1}NH ($\Delta\delta/\Delta t$ = −8.0 ppb/K) were reduced to 25%. The purpose of this manipulation is to mimic solvent surrounding in in vacuo calculation by experimental data.[12h]

A harmonic restraint potential was employed for upper and lower distance bounds. The distance restraints function switches from harmonic to linear, when the deviation is greater than 10% from the target distance. The lower bound distances are given in Table IV, obtained from averaging over both sides of the diagonal; for the upper bounds, 100 and 90 pm were added for each methyl and nonstereospecifically assigned CH_2 group, respectively, except for NH–NH distances, as noted above.[42b]

The starting structure for I was minimized (conjugate gradient algorithm[49]) for 1000 steps. Then 1000 steps restrained EM (K_{dc} = 5000 kJ mol^{-1} nm^{-2}) with SHAKE[50] were performed. The resulting structure EMI was used as the input structure for different MD simulations. The minimization of II with the same protocol lead to structure EMII.

The MD simulations were performed with the SHAKE procedure; a step size of 2 fs for the numerical integration of Newton's equation (leap-frog algorithm[50]) was reasonable.

Refinement Protocol of I. Before averaging over a trajectory, a time span of 10 ps was used to equilibrate the system. Initial velocities for the atoms were taken from a Maxwellian distribution at the corresponding temperature. During the first 1 ps, the system was strongly coupled to a 1000 K temperature bath[48] with a temperature relaxation time τ of 0.01 ps and a force constant for the distance restraints of 4000 kJ mol^{-1} nm^{-2} (K_{dc}). In the next 4 ps, the temperature was scaled down to 300 K and the temperature relaxation time was increased to 0.1 ps; the system was now weakly coupled to the temperature bath. Simultaneously the value for K_{dc} was decreased to 2000 kJ mol^{-1} nm^{-2}. The next 5 ps was used for equilibration of the system. The resulting structure served as the starting structure for recording a trajectory over a 40-ps time span with K_{dc} = 2000 kJ mol^{-1} nm^{-2}. During the next 5 ps, the force constant was reduced to 1000 kJ mol^{-1} nm^{-2}; this period was likewise used as an equilibrium period. A 40-ps trajectory was recorded with this reduced force constant (structure MDI^a). This procedure (5-ps equilibrium, 40-ps dynamics) was then repeated without applying any constraints.

When distance constraints with different force constants K_{dc} are applied, the peptide backbone angles show no large fluctuations. Free MD without distance constraints reveal the tendency of the saccharide unit to compensate its charges by adopting a structure that conflicts with the NMR data.

The final structure MDI^a (averaged over MD simulation) now satisfied 54 distance constraints, while violating 3 NOE distances (Table IV, underlined in Table X). The violations may arise from errors in the experimental parameters. However, in many instances, conformational mobility in the molecule was the cause of such errors,[51,52] and it was possible to determine these conformations by use of MD simulations, for example, in the case of the cyclic decapeptide antamanide.[31]

Our results for I and II show that the observed NOE data set (including the complete diastereotopic assignment) cannot be satisfied by one conformation; at least two conformations are required. Most of the diastereotopically assigned NOE's are fulfilled so that the fixing of the side chain dihedrals as described before does not produce an error (MD simulations in vacuo without fixing side chains in preferred conformations lead to a physically unrealistic picture due to vacuum effects). But in one case (Phe^{5}NH–C$_\beta H$'s) the deviation from the calculated distance to the measured one is larger. The relevant NMR parameters (NOE and coupling constants) depend in a nonlinear way on distances and dihedral angles;[51] short distances are overemphasized by NOE's. It turned out that there is a fast conformational equilibrium between two (or more) conformations which differ in a flip about the φ and ψ dihedral angles around the amide bond between Gln^4 and Phe^5; this flip caused two different β-turn structures.

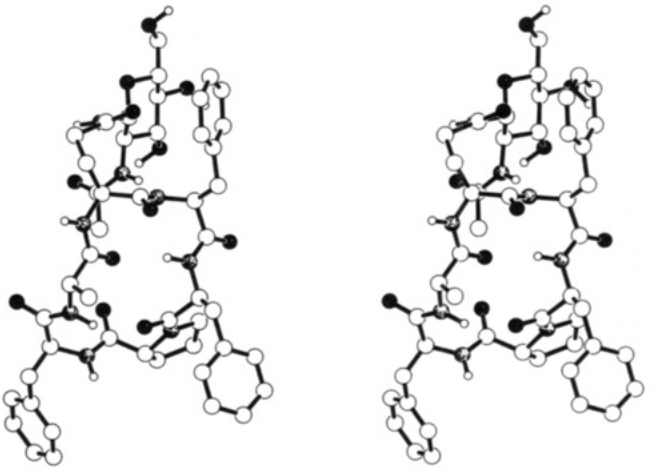

Figure 3. Stereoview of the mean structure of Peptide I with a βII-turn in the Ala^3 to Phe^6 region, obtained from averaging the 40-ps trajectory from MDI^a (in vacuo). The protons bound to carbon are not shown.

Therefore, we performed in vacuo simulations in a similar manner with different starting conformation (with a βI-turn between Ala^3 and Phe^6, corresponding to a 180° flip about the Gln^4–Phe^5 bond). The structure after energy minimization was equilibrated for 5 ps at 300 K with a force constant K_{dc} = 1000 kJ mol^{-1} nm^{-2}; then a trajectory over 40 ps with the same force constant was performed. Two NOE's that cannot be satisfied by a βI-turn structure in this moiety were omitted from the distance constraint list (marked in Table X).

The distance constraints previously in violation were satisfied by the new averaged conformation MDI^b (MD trajectory over 40 ps). During the simulation, no conformational change occurred. If we calculate the NMR parameters (NOE data) from both trajectories MDI^a and MDI^b (average restraint violation 11 and 10 pm for MDI^a and MDI^b, respectively) under the assumption that both conformations are equally populated ($p_a = p_b = 0.5$), all NOE distances are satisfied (average restraints violation 9 pm) and the large deviation of some NOE's vanishes.

The total potential energy of these simulations (as averaged over the 40-ps trajectory) is given in Table X. The values for the distance restraint energies are also given, but a comparison of the energies naturally suffers from the different numbers of distance constraints applied.

For both structures, the βII′-turn in the other peptide moiety was not affected from the occurrence of the β-turn on the counterside of the peptide.

The two different structures shown in Figures 5 and 6 were obtained by averaging over the trajectories and energy minimized for five steps with the same force constant as applied in the trajectory to relax them from physically unrealistic averaging artifacts. The average dihedral angles and observed hydrogen bonds for both structures are given in Tables VI and VIII, respectively.

MD Simulation with Time-Dependent Distance Constraints. To confirm the model of two fast interconverting conformers in I, MD simulations using time-dependent distance restraints[53] were

(49) (a) Fletcher, R.; Reeves, C. M. *Comput. J.* **1964**, *7*, 149–154. (b) van Gunsteren, W. F.; Karplus, M. *Comput. Chem.* **1980**, *7*, 266–274.

(50) (a) Ryckaert, J. P.; Cicotti, C.; Berendsen, H. J. C. *J. Comput. Phys.* **1977**, *23*, 327–343. (b) van Gunsteren, W. F.; Berendsen, H. J. C. *Mol. Phys.* **1977**, *34*, 1311–1327.

(51) Jardetzki, O. *Biochim. Biophys. Acta* **1980**, *621*, 227–232.

(52) Scarsdale, J. N.; Yu, R. K.; Prestegard, J. H. *J. Am. Chem. Soc.* **1986**, *108*, 6778–6784.

(53) (a) Torda, A. E.; Scheek, R. M.; van Gunsteren, W. F. *Chem. Phys. Lett.* **1989**, *157*, 289–294. (b) Torda, A. E.; Scheek, R. M.; van Gunsteren, W. F. *J. Mol. Biol.* **1990**, *214*, 223–235.

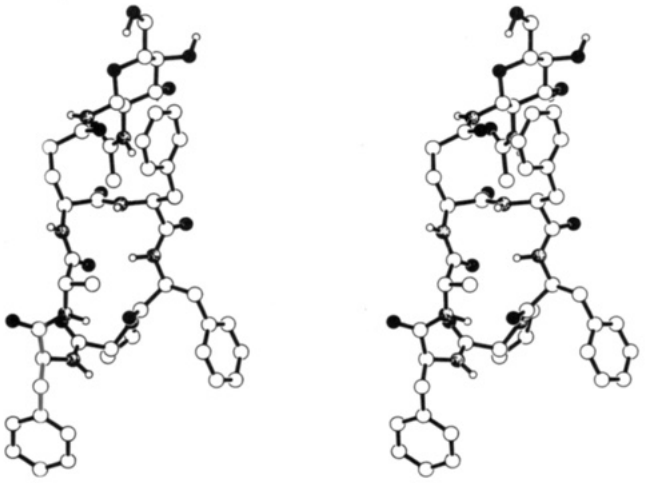

Figure 4. Stereoview of the mean structure of Peptide I with a βI-turn in the Ala[3] to Phe[6] region, obtained from averaging the 40-ps trajectory from MDI[b] (in vacuo). The protons bound to carbon are not shown.

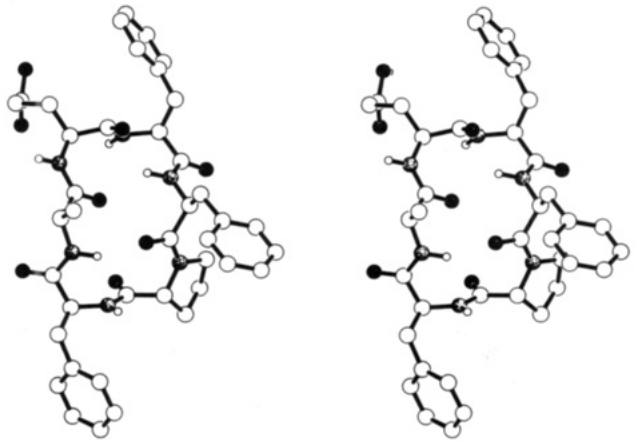

Figure 5. Stereoview of the mean structure of Peptide II with a βII-turn in the Ala[3] to Phe[6] region, obtained from averaging the 40-ps trajectory from MDII[a] (in vacuo). The *tert*-butyl protecting group (not included in calculation) and the protons bound to carbon are not shown.

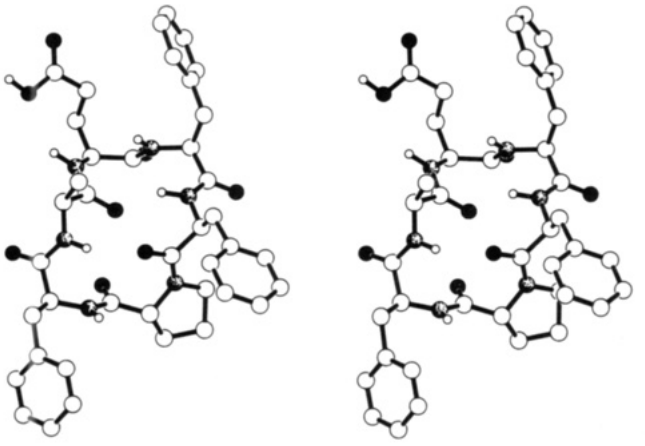

Figure 6. Stereoview of the mean structure of Peptide II with a βI-turn in the Ala[3] to Phe[6] region, obtained from averaging the 40-ps trajectory from MDII[b] (in vacuo). The *tert*-butyl protecting group (not included in calculation) and the protons bound to carbon are not shown.

carried out. This method performs a wider search of conformational space. The NOE data set is not treated as a static additional potential in the force field, but a term is included so that the distance constraints must only be satisfied as a $\langle r^{-3}\rangle^{-1/3}$ weighted time average over a simulated trajectory. A better approximation of the physical nature of the NOE's is achieved that will reflect the conformational equilibrium.[53] Therefore, this method gives a better estimation of the conformational behavior of a flexible molecule in solution.

Table VI. Comparison of the MD-Calculated Backbone, Side Chain, and Saccharide Dihedrals (deg) of Glycopeptide I Obtained from Several MD Simulations[a]

	dihedral angle	MDI[a]	MDI[b]	MDI[c]
D-Pro[1]	φ	62.6 (8.9)	62.2 (9.5)	67.4 (16.1)
	ψ	−117.1 (11.1)	−113.3 (10.8)	−118.4 (19.2)
	χ_1	−15.3 (21.4)	6.6 (23.0)	−9.4 (24.5)
	ω	177.1 (5.2)	179.0 (5.8)	176.3 (8.4)
Phe[2]	φ	−78.5 (14.9)	−72.2 (11.8)	−83.6 (21.0)
	ψ	−16.1 (14.8)	−18.6 (16.2)	2.8 (38.1)
	χ_1	−60.2 (1.9)	−60.1 (1.6)	−60.3 (1.0)
	ω	175.5 (7.5)	172.5 (7.4)	174.8 (12.2)
Ala[3]	φ	−100.0 (19.8)	−104.9 (17.8)	−121.5 (44.0)
	ψ	157.0 (10.1)	154.7 (9.8)	151.7 (32.9)
	ω	176.1 (7.5)	−178.5 (7.7)	178.9 (12.0)
Gln[4]	φ	−60.3 (10.7)	−48.2 (10.9)	−59.4 (36.1)
	ψ	110.7 (8.9)	−42.8 (10.3)	48.4 (74.3)
	χ_1	−127.2 (12.4)	−175.2 (9.4)	−141.8 (48.4)
	χ_2	−64.1 (8.7)	−81.5 (9.0)	33.9 (114.3)
	χ_3	130.2 (15.9)	143.9 (15.6)	−140.4 (68.3)
	ω	−179.7 (5.5)	177.4 (4.8)	154.6 (56.8)[b]
Phe[5]	φ	98.2 (13.6)	−74.1 (11.6)	−166.1 (89.3)
	ψ	−33.2 (14.8)	−31.0 (9.6)	61.5 (145.6)
	χ_1	−60.3 (1.5)	−60.2 (1.4)	−60.3 (1.4)
	ω	−176.9 (7.3)	−172.8 (7.3)	−178.0 (13.3)
Phe[6]	φ	−124.0 (15.7)	−158.8 (11.8)	132.7 (150.9)
	ψ	105.8 (10.6)	118.1 (10.9)	113.2 (18.0)
	χ_1	179.9 (1.5)	−179.8 (1.7)	−179.7 (1.3)
	ω	−175.1 (7.0)	172.7 (6.3)	176.8 (10.9)
glycos	C_γ–C_δ–N_δ–C^1	−170.0 (7.0)	−173.5 (8.7)	−177.9 (13.5)
	O^5–C^1–N_δ–C_δ	−101.6 (18.3)	−93.3 (18.4)	−127.5 (28.9)
	C_δ–N_δ–C^1–C^2	140.2 (21.7)	145.5 (18.1)	112.1 (28.0)
GlcNAc	N^2–C^2–C^3–C^4	−178.2 (11.5)	−178.9 (10.7)	−176.7 (14.8)
	C^4–C^5–C^6–O^6	−149.7 (46.8)	166.0 (44.3)	177.4 (64.3)
	C^2–N^2–C'–CH_3	176.3 (8.7)	176.6 (8.8)	−179.9 (9.7)
	N_δ–C^1–O^5–C^5	172.5 (7.6)	172.4 (7.6)	174.4 (9.4)
	N_δ–C^1–C^2–C^3	−177.2 (7.2)	−177.5 (7.6)	178.6 (11.5)
	O^5–C^1–C^2–C^3	60.8 (7.7)	61.0 (7.3)	58.2 (11.0)
	C^1–C^2–C^3–C^4	−53.3 (9.9)	−53.7 (9.1)	−49.9 (12.9)
	C^2–C^3–C^4–C^5	48.8 (12.9)	49.3 (9.4)	46.4 (13.6)
	C^3–C^4–C^5–O^5	−51.0 (9.6)	−51.0 (9.5)	−50.6 (12.2)
	C^4–C^5–O^5–C^1	60.0 (7.9)	60.2 (8.6)	60.9 (8.9)
	C^5–O^5–C^1–C^2	−65.7 (7.0)	−65.9 (7.0)	−65.1 (8.3)
	C^3–C^2–N^2–C'	−198.1 (17.6)	−101.3 (16.3)	−63.5 (66.3)

[a] The numbers in parentheses denote the rms fluctuation obtained by averaging. The ω dihedrals are given to the next amino acids. [b] The large observed deviation from planarity is due to averaging over different conformations in MDI[c] by using time-dependent distance constraints. The large rms fluctuation reflects the flexibility in this region. For details, see text.

The EMI structure was used as a starting structure; the integration time step was set to 2 fs. For the simulations with the time-averaged distance restraints, the required initial value was set for each restraint to be 20 pm less than the experimental value. The artificial force is therefore gradually increased for those restraints that have the greatest violation.[53b] The time constant τ for the decay of the "memory function" was set to 2.5 ps.[54] This value directly affects the rate of motion during the simulation and therefore influences the time requirements for the averaging.[53b] After an initial 10-ps time span for equilibrium (without time-dependent distance restraints), a 90-ps MD simulation in vacuo was started with K_{dc} = 1000 kJ mol^{-1} nm^{-2}.

The observation of two or more fast interconverting conformers could be confirmed after analyzing the trajectory. The distances (Table IV), dihedral angles (Table VI), and the corresponding $^3J_{NH,C\alpha H}$ coupling constants (Table II), were calculated as an average over all produced different conformations. The average restraint violation (over 57 NOE's) for this simulation is smaller (9 pm) than for simulations without enforcing the distance restraints as a time average; it is in the same range as when averaging over the different conformations (as described above).

The calculated proton–proton distances now agree better with experimentally derived values. The NOE's involving Phe[5]N*H* are

(54) Torda, A. E. Personal communication.

Table VII. Comparison of the MD-Calculated Backbone and Side Chain Dihedrals (deg) of the Cyclic Hexapeptide II Obtained from Several MD Simulations[a]

	dihedral angle	MDII[a]	MDII[b]
D-Pro[1]	φ	62.0 (10.3)	60.4 (10.2)
	ψ	−115.0 (11.1)	−111.8 (11.9)
	χ_1	−4.7 (25.1)	3.6 (25.8)
	ω	179.6 (5.8)	179.7 (6.1)
Phe[2]	φ	−84.7 (16.9)	−70.6 (17.0)
	ψ	−11.0 (24.0)	−28.4 (17.3)
	χ_1	−60.1 (1.5)	−60.1 (1.1)
	ω	175.3 (7.6)	175.5 (8.0)
Ala[3]	φ	−106.8 (25.9)	−101.9 (19.0)
	ψ	162.7 (11.9)	123.4 (33.3)
	ω	177.3 (7.6)	−178.1 (8.3)
Glu[4]	φ	−54.4 (12.9)	−5.9 (42.8)
	ψ	114.3 (12.1)	−55.3 (29.7)
	χ_1	−91.5 (29.0)	62.2 (11.4)
	χ_2	−66.2 (12.5)	−126.2 (57.6)
	χ_3	−127.4 (81.2)	170.8 (352.5)
	ω	−178.1 (6.5)	177.8 (5.7)
Phe[5]	φ	83.0 (13.5)	−83.7 (24.1)
	ψ	−28.6 (21.1)	−30.5 (16.1)
	χ_1	−60.1 (1.6)	−60.0 (1.8)
	ω	−177.4 (7.4)	−178.4 (8.7)
Phe[6]	φ	−122.3 (16.1)	−136.3 (21.4)
	ψ	105.4 (14.0)	108.2 (14.2)
	χ_1	−179.6 (1.7)	−179.8 (1.8)
	ω	175.1 (7.9)	175.5 (8.6)

[a] The numbers in parentheses denote the rms fluctuation obtained by averaging. The ω dihedrals are given to the next amino acids.

better represented during the time scale of the simulation due to the greater flexibility allowed (see for example the three underlined NOE's in Table X). The distance for Phe[5]N*H*–Ala[3]C$^{\beta}$*H* is not in the allowed range of 322–422 pm (this is only possible during the MDI[b] simulation), but the calculated values for the MDI[c] and MDI_{av} are 80–90 pm smaller than for the MDI[a] simulation and show only a deviation of 50–65 pm from the accepted values. The same observations have been made for the other two distances not satisfied in simulation MDI[a].

The distance restraint energy for MDI[c] is lower than for MDI[a] (both calculated with 57 distance restraints), showing the advantage of the application of time-dependent distance constraints. The corresponding energy for MDI[b] is calculated for only 55 distance restraints and therefore cannot be compared to the other values. Considering the accuracy of NOE-derived distance restraints, these approaches produce satisfactory agreement, showing the effectiveness of the new refinement technique for peptides with internal flexibility.

With the $^3J_{NH,C\alpha H}$ coupling constants are calculated as statistical averages over different conformations, the calculated values $\langle {}^3J_{calcd}\rangle^{av}$ (for averaging over two conformations) and $\langle {}^3J_{calcd}\rangle^{c}$ (with time-dependent distance constraints) reveal good agreement with experimental data (Table II). The deviation between calculated and experimental values is larger than 1.8 Hz only for Phe[6]. The calculated J values from MDI[a]/MDI[b] cannot fulfill the experimentally derived data as well as when averaging over both conformations, especially when the corresponding dihedral angles are located in backbone regions, which are involved in the dynamic flexibility.

Hence, the interpretation of coupling constants has to be done carefully. A situation with different conformers in dynamic equilibrium, as we have described here, can lead to substantial errors when determining the geometry of reverse turns. The calculation of corresponding dihedral angles is only possible, if these NMR data reflect the conformational behavior of a single conformation. Therefore, coupling constants, often mentioned in the literature as main argument for determination of β-turn geometries, are in some cases not sufficient to reveal conformational properties because of conformational averaging, which cannot be excluded without performing MD calculations.

After the positional rms fluctuations for the heavy atoms (data not given) or the torsion angle rms fluctuations were analyzed (Table VIII), it was obvious that, for the time-averaged forces, the fluctuations are consistently larger. The rms fluctuations observed of the torsion angles for the βII′-turn (D-Pro[1]–Phe[2]) are not significantly larger (1.5–2.0). The fluctuation of the Ala[3] φ angle has increased, in the flexible peptide region, and a large increase of Gln[4] φ/ψ, Phe[5] φ/ψ, and Phe[6] φ angle fluctuations is observed. This illustrates interconversion of different conformations and therefore the larger available conformational space of the structure resulting from this simulation.

The Gln[4] side chain, connecting the saccharide to the peptide unit, shows a greater flexibility; this observation may arise from the increased backbone mobility and the conformational equilibrium.

The glycosidic bond is as flexible as without use of time-averaged restraints. The same observation is made for the carbohydrate geometry except the C[3]–C[2]–N[2]–C′ angle, connecting the

Table VIII. Hydrogen Bonds in the Glycopeptide I from Different MD Calculations[a]

		MDI[a]				MDI[b]				MDI[s1]				MDI[c]			
donor	acceptor	Θ_{DH-A}	d_{D-A}	%	type	Θ_{DH-A}	d_{D-A}	%	type	Θ_{DH-A}	d_{D-A}	%	type	Θ_{DH-A}	d_{D-A}	%	type
Phe[5]NH	Ala[3]C=O	125.0	292	6.3	γi	–	–	–	–	128.6	288	10.0	γi	139.3	288	17.1	–
Phe[6]NH	Gln[4]C=O	134.9	327	67.3	γ	–	–	–	–	137.0	315	49.0	γ	139.3	306	21.1	–
Phe[6]NH	Ala[3]C=O	141.6	294	68.8	βII	151.2	290	97.0	βI	147.3	299	69.0	βII	152.7	301	63.3	βI/βII
Ala[3]NH	Phe[6]C=O	151.1	302	96.8	βII′	152.8	305	97.3	βII′	144.6	306	93.0	βII′	148.4	311	67.1	βII′
Ala[3]NH	D-Pro[1]C=O	130.1	312	5.0	γi	130.2	306	3.5	γi	133.0	308	8.0	γi	139.5	306	26.0	γi
Gln[4]N$_\delta$H	GlcNAcC=O	134.3	348	11.0	–	136.9	356	10.3	–	136.0	333	7.0	–	143.8	324	5.7	–
GlcNAcO[3]H	GlcNAcO[7]	143.5	330	13.5	–	140.9	327	18.5	–	–	–	–	–	140.2	319	11.1	–
GlcNAcO[4]H	GlcNAcO[6]	133.8	298	3.3	–	–	–	–	–	–	–	–	–	–	–	–	–
GlcNAcN[2]H	Glc[4]C=O	–	–	–	–	138.6	317	50.5	–	–	–	–	–	–	–	–	–
GlcNAcO[4]H	GlcNAcO[3]	–	–	–	–	–	–	–	–	123.6	273	3.0	–	–	–	–	–
Phe[5]NH	GlcNAcO[5]	–	–	–	–	–	–	–	–	–	–	–	–	142.8	335	6.1	–
Gln[4]NH	GlcNAcO[7]	–	–	–	–	–	–	–	–	–	–	–	–	137.5	343	4.2	
GlcNAcOH[6]	Phe[5]C=O	–	–	–	–	–	–	–	–	–	–	–	–	139.7	319	5.8	–
GlcNAcN[2]H	Gln[4]C[δ]=O	–	–	–	–	–	–	–	–	–	–	–	–	135.9	313	22.6	–

Three-Center Hydrogen Bonds in the Glycopeptide I

		MDI[a]			MDI[b]			MDI[s1]			MDI[c]		
donor	acceptor 1 acceptor 2	Θ_{DH-A1} Θ_{DH-A2}	d_{D-A1} d_{D-A2}	$\%_{all}$	Θ_{DH-A1} Θ_{DH-A2}	d_{D-A1} d_{D-A2}	$\%_{all}$	Θ_{DH-A1} Θ_{DH-A2}	d_{D-A1} d_{D-A2}	$\%_{all}$	Θ_{DH-A1} Θ_{DH-A2}	d_{D-A1} d_{D-A2}	$\%_{all}$
Phe[6]NH	Ala[3]C=O	137.2	298		–	–	–	131.0	302		143.4	299	
	Gln[4]C=O	129.5	331	20.0				129.3	308	15.0	131.4	328	3.7
Ala[3]NH	Phe[6]C=O	138.5	307		–	–	–	135.5	308		138.7	313	
	D-Pro[1]C=O	127.1	316	3.5				127.7	319	5.0	130.1	319	6.6

[a] Only hydrogen bonds with an occurrence greater than 3% are displayed. The criterion for a hydrogen bond is the donor hydrogen–acceptor angle must be larger than 90° and the distance d_{H-A} from hydrogen to acceptor smaller than 250 pm.

acetamido function to the saccharide ring system.

Hence, we assume that the MDI[a] and MDI[b] structures are the major populated conformers in the fast dynamical equilibrium. The course of interconversion and the available conformational space are reflected during the MDI[c] simulation.

Conformation of the Glycosidic Bond and the Saccharide Unit. The conformations of the N-glycosidic linkage and saccharide moiety are identical in both conformers. The observed trans orientation of Gln^{4}N$_\delta H$ and GlcNAc-C^1H indicated by a weak NOE (288 pm) was represented in the MD simulations with a dihedral angle C$_\delta$–N$_\delta$–C^1–C^2 of 140.2° (21.7) for MDI[a], 145.5° (18.1) for MDI[b], and 112.1° (28.0) for MDI[c]. The values in parentheses indicate the rms fluctuation obtained by averaging.

These values are in agreement with data from the literature. An X-ray analysis of GlcNAc bound to an asparagine residue reveals the same conformational properties of the glycosidic linkage and of the sugar conformation.[55] As a model compound for the N-glycosidic linkage, 1-*N*-Acetyl-β-D-glucopyranosylamine was analyzed by X-ray and circular dichroism, and the proposed trans orientation for the C^{1}H proton of the sugar and the amide proton was confirmed.[56] This preferred orientation was also previously described for crystalline β-D-GlcNAc-N–Asn.[55] X-ray analysis has shown that the glucopyranose rings of GlcNAc-N-Asn and Glc-N-Asn both have the $^4C_1$ conformation. The glycosidic torsion angles C′–N$^{1\prime}$–C^1–C^2 (in our definition, C$_\delta$–N$_\delta$–C^1–C^2) are 141.0° and 157.6° for both of these compounds, corresponding well to our obtained values (see above and Table VI). A trans orientation is also proposed for this glycosidic linkage in larger complex-type oligosaccharides linked to asparagine from the analysis of CD measurement and NMR coupling constants analysis.[57]

Not only the glycosidic bond is trans oriented but also the N^{2}H bond of the amide at C^2 is trans oriented to the C^{2}H bond in GlcNAc-N-Asn. The corresponding C^3–C^2–N^2–C′ angle was given in the literature to be −125.6°.[55a] We observed values of −108.1° (17.6) and −101.3° (16.3) (for MDI[a] and MDI[b], respectively). The values are in the same range but differ from the simulation with time-dependent distance constraints (−66.5° (66.3)). Here the torsion angle and rms fluctuation reveal a large mobility around the corresponding C^2–N^2 bond. Two short distances from GlcNAcN^2H to protons on opposite sides of the six-membered ring system (to GlcNAc-H^1 and to GlcNAc-H^2) were observed and cannot be fulfilled by one rigid conformation of the acetamido group relative to the saccharide. A high violation of these NOE's in all trajectories, except for the final one with time-dependent distance constraints MDI[c], was observed. These results reflect the internal dynamics in the GlcNAc moiety; the violated distances involving Glc*N*Ac-N^{2}H show a better agreement to experimental data. The largest observed deviation is 89 pm for the distance GlcNAc-N^{2}H to Gln^{4}C$_\gamma$H (experimental 247–337 pm, not diastereotopically assigned; calculated 426 pm). This insufficient agreement between experiment and calculation may arise from the increased flexibility of the acetamido group as reflected in our calculations. Therefore, the assumption of isotropic mobility for the correct interpretation of NOE effects may lead to substantial errors for that part of the molecule. However, all other experimental data are in accord with the results from simulation.

The conformation of the saccharide subunit, a $^4C_1$ chair conformation of the six-membered heterocyclic ring system with all substituents in equatorial position, is also in agreement with previously published results. A force field calculation of β-D-glucose[58] suggests that such monosaccharides may undergo changes in their ring conformation with a rotation of up to 10° in the dihedral angle but with almost no change in energy. The $^1C_4$ conformation is calculated to have a higher energy content (about 3 kcal/mol) than the $^4C_1$ conformation. The dihedral angles describing the D-glucose ring conformation obtained from previously described MD simulations correspond well with our results.[59]

MD Simulation of I in Aqueous Solution. The averaged MDI[a] (with a βII-turn in the region between Ala^3 and Phe^6) was minimized as described in vacuo and put in a box of 545 water molecules in order to test the stability and dynamical properties of the resulted structures. These simulations were performed in water because of a lack of a reliable DMSO force field at this time. Although no experimental data from measurements in water were available, these simulations will better reflect the "realistic" measurement conditions in solution.

A truncated octahedron with a volume of 17.3 nm^3 was used.[60] The water molecules are modeled by the simple rigid three-point charge model (SPC) as described in the literature.[61] All calculations in water were performed without applying the SHAKE procedure; the time step for integration was reduced to 1 fs. A cutoff radius of 1 nm for the calculation of the nonbonded interactions was used.

The solvent was allowed to relax by 500 steps of EM while the position of the solute atoms was kept fixed by applying a harmonic position restraining potential. The position restraining potential was removed, and another 500 steps of EM was carried out. For both minimizations, no distance restraints were applied. Two MD simulations were performed at 300 K, the first with K_{dc} = 1000 kJ mol^{-1} nm^{-2} for 20 ps (structure MDI[s1]), the second with no distance restraints for 80 ps.

The stability of the βII-type conformer in water was confirmed not only during a time span of 20 ps with application of distance constraints, but also without any constraints. No conformational changes could be detected in water; this observation is in contradiction with results from in vacuo simulations. While examination of the in vacuo simulation without distance constraints suggests the glycopeptide to be a relatively flexible molecule, this flexibility could not be confirmed during simulation in water. These observations can suffer from the applied short simulation times (80 ps) due to the high viscosity of the solvent; a detailed description of conformational behavior in solution is not possible. Nevertheless, the observation of some conformational transitions was often observed during short simulation periods in water.[62]

Refinement Protocol of II. The conformational analysis of II, the building of the crude model structure, and refinement produced similar results as found for I.

All simulations for II were performed in vacuo. With the minimized structure EMII, a 10-ps time span for equilibration with K_{dc} = 4000 kJ mol^{-1} nm^{-2} was used during the first 1 ps, K_{dc} = 2000 kJ mol^{-1} nm^{-2} during the next 4 ps, and K_{dc} = 1000 kJ mol^{-1} nm^{-2} during the next 5 ps. With the resulting structure, a trajectory over a time span of 40 ps was recorded. The temperature relaxation time and all other parameters were treated as described before.

As for the glycopeptide, not all NOE's could be satisfied by assuming only one conformation. Therefore, we have chosen the same approach as for the refinement of I.

(i) Two simulations were performed with restraining of the side chain χ_1 dihedrals (full diastereotopic assignment of all NOE data) starting from alternate conformations with βII-turn or βI-turn between Ala^3 and Phe^6; the resulting structures were named MDII[a] and MDII[b], respectively.

(ii) Calculation of the NMR parameters (NOE data) from both trajectories was performed under the assumption that both conformations are equally populated.

Also in this case we omitted two NOE's, which cannot be satisfied by a conformation including a βI-turn between Ala^3 and

(55) (a) Delbaere, L. T. *J. Biochem. J.* **1974**, *143*, 197–205. (b) Ohannessian, J.; Avenel, D.; Neuman, A.; Gillier-Pandrand, H. *Carbohydr. Res.* **1980**, *80*, 1.
(56) Bush, C. A.; Blumberg, K. *Biopolymers* **1982**, *21*, 1971.
(57) Bush, C. A.; Dua, V. K.; Ralapati, S.; Warren, C. D.; Spik, G.; Strecker, G.; Montreuil, J. *J. Biol. Chem.* **1982**, *257*, 8199.
(58) Rao, V. S. R.; Joshi, N. V. *Biopolymers* **1979**, *18*, 2993.
(59) (a) Brady, J. W. *J. Am. Chem. Soc.* **1986**, *108*, 8153–8160. (b) Brady, J. W. *J. Am. Chem. Soc.* **1989**, *111*, 5155–5165.
(60) Adams, D. J. *J. Chem. Phys. Lett.* **1979**, *62*, 329–332.
(61) Berendsen, H. J. C.; Postma, J. P. M.; van Gunsteren, W. F.; Hermans, J. In *Intermolecular Forces*; Pullman, B., Ed.; Reidel: Dordrecht, The Netherlands, 1981; pp 331–342.
(62) Kessler, H.; Wein, T. *Liebigs Ann. Chem.* **1990**, 179–184.

Table IX. Hydrogen Bonds in the Cyclic Hexapeptide II from Different MD Calculations[a]

donor	acceptor	MDII[a] Θ_{DH-A}	MDII[a] d_{D-A}	MDII[a] %	MDII[a] type	MDII[b] Θ_{DH-A}	MDII[b] d_{D-A}	MDII[b] %	MDII[b] type
Phe^{5}NH	Ala^{3}C=O	–	–	–	–	132.5	256	7.0	γ
Phe^{6}NH	Glu^{4}C=O	139.2	300	73.0	γ	–	–	–	–
Phe^{6}NH	Ala^{3}C=O	143.1	297	59.5	βII	155.2	288	91.8	βI
Ala^{3}NH	Phe^{6}C=O	148.2	308	90.0	βII′	150.6	308	90.8	βII′
Ala^{3}NH	D-Pro^{1}C=O	132.7	322	12.5	γi	–	–	–	–
Phe^{5}NH	Glu^{4}C$_\delta$O^1	136.5	258	4.0	–	147.6	356	10.8	–
Phe^{5}NH	Glu^{4}C$_\delta$O^2	138.9	347	3.3	–	144.6	342	9.3	–
Glu^{4}NH	Phe^{2}C=O	–	–	–	–	132.4	331	17.5	γi
Glu^{4}NH	Glu^{4}C$_\delta$O^1	–	–	–	–	140.4	323	20.5	–
Glu^{4}NH	Glu^{4}C$_\delta$O^2	–	–	–	–	142.5	330	9.0	–

Three-Center Hydrogen Bonds in the Cyclic Hexapeptide II

donor	acceptor 1 / acceptor 2	MDII[a] Θ_{DH-A1} / Θ_{DH-A2}	MDII[a] d_{D-A1} / d_{D-A2}	MDII[a] $\%_{all}$	MDII[b] Θ_{DH-A1} / Θ_{DH-A2}	MDII[b] d_{D-A1} / d_{D-A2}	MDII[b] $\%_{all}$
Phe^{6}NH	Ala^{3}C=O	135.3	297		–	–	–
	Glu^{4}C=O	131.5	301	22.5			
Ala^{3}NH	Phe^{6}C=O	138.4	315		–	–	–
	D-Pro^{1}C=O	130.2	325	8.0			

[a] Only hydrogen bonds with an occurrence greater than 3% are displayed. The criterion for a hydrogen bond is the donor hydrogen–acceptor angle must be larger than 90° and the distance d_{H-A} from hydrogen to acceptor smaller than 250 pm.

Phe^6. The results for the NOE's with the largest violation are given in Table X.

The resulting structures for both conformers are given in Figures 5 and 6; each is obtained after averaging over a 40-ps time span and 5 steps of EM (with the same K_{dc} as in the simulation). The comparison between experimental and calculated distances, the dihedral angles, and the hydrogen bonds are given in Tables V, VII, and IX, respectively.

Comparison of the Structures for the Glycopeptide and the Cyclic Hexapeptide. It has been shown that N-glycosylation does not affect the conformation or the overall shape of the peptide backbone or side chains. A fast dynamical interconversion between two major conformers in equilibrium differing by the type of the β-turn was observed for both compounds.

Comparison of the two different hexapeptide conformers with the corresponding glycopeptide conformers shows a great similarity. The dihedral angles of the different peptide conformers are identical with the corresponding glycopeptide conformers. The comparison of the glutamic acid to the glutamine in the glycopeptide shows the greatest deviations caused by the lack of NOE-derived distance data for the fixing of this side chain; therefore, an exact structural analysis of this side chain conformation in II is impossible.

We could not observe any change of the peptide backbone structure, conformation of side chains, hydrogen-bonding pattern, or fast dynamical equilibrium caused by N-glycosylation. A quite similar set of NOE data leads after MD refinement of the crude structures to the same set of two backbone conformers for I and II, respectively.

A comparison between the molecular mobility during the MD simulations of I and II (positional or torsion angle rms fluctuations) further shows that N-glycosylation has no significant effect on the peptide backbone mobility. Comparing MDI[b] with MDII[b], only the Glu^4 φ/ψ angles show increased mobility (3–4 times). All other fluctuations are in the same range. This is also observed from the comparison of the simulation MDI[a]/MDII[a]. The mobility of the Gln^4 side chain decreased when compared with the Glu^4 mobility in the cyclic hexapeptide, but this effect seems to be an artifact from applying different distance constraints for the side chains.

Table X. Comparison of Experimental and Calculated Proton–Proton Distances (pm) for I and II, Which Deviate Most from the Obtained Different Conformations[a]

Compound I

involved protons		NOESY	MDI[a]	MDI[b]	MDI$_{av}$	MDI[c]
Phe^{5}N*H*	Phe^{5}C$_\alpha$*H*	244	213	270[d]	242	252
Phe^{5}N*H*	Gln^{4}C$_\alpha$*H*	231	193	344[d]	269	272
Phe^{5}N*H*	Ala^{3}C$_\beta$*H*	322[b]	*565*	389	477	483
Phe^{5}N*H*	Phe^{5}C$_\beta$*H*$^{pro-R}$	267	*367*	245	306	293
Phe^{5}N*H*	Phe^{5}C$_\beta$*H*$^{pro-S}$	338	*408*	350	379	374
Phe^{5}N*H*	Gln^{4}C$_\beta$*H*	283[c]	398	323	361	378
Phe^{5}N*H*	Gln^{4}C$_\gamma$*H*	407[c]	435	460	448	468
Phe^{5}C$_\alpha$*H*	Phe^{5}C$_\beta$*H*$^{pro-S}$	244	241	245	243	242
Phe^{5}C$_\alpha$*H*	Phe^{5}C$_\beta$*H*$^{pro-R}$	283	286	290	288	287
average restraint violation		–	11	10	9	9
total potential energy		–	303.13	284.46	–	324.18
energy of distance restraints		–	57.03	35.78	–	45.95

Compound II

involved protons		NOESY	MDII[a]	MDII[b]	MDII$_{av}$
Phe^{5}N*H*	Phe^{5}C$_\alpha$*H*	240	207	274[d]	240
Phe^{5}N*H*	Glu^{4}C$_\alpha$*H*	239	200	337[d]	269
Phe^{5}N*H*	Phe^{5}C$_\beta$*H*$^{pro-R}$	261	358	251	304
Phe^{5}N*H*	Phe^{5}C$_\beta$*H*$^{pro-S}$	397	*373*	355	377
Phe^{5}N*H*	Glu^{4}C$_\beta$*H*	342[c]	382	356	369
average restraint violation		–	9	10	8
total potential energy		–	275.52	280.42	–
energy of distance restraints		–	19.68	14.04	–

[a] For the notation of the different MD trajectories, please see text. For each simulation, the average restraint violation (pm), the total potential energy $E_{tot\ pot}$ (kJ mol^{-1}), and the energy of the distance restraints E_{dis} (kJ mol^{-1}) are denoted, obtained by averaging over the corresponding simulations. [b] Increased by 100 pm for MD run (CH_3 group (ref 42b)). [c] Increased by 90 pm for MD run (CH_2 without diastereotopic assignment (ref 42b)). [d] NOE's omitted in the MD runs MDI[b] and MDII[b] (see text).

Experimental Section

a. Synthesis. General Procedures. The protected amino acid derivatives were prepared as described in the literature. All intermediates were characterized by TLC, melting point, specific rotation, and ^{1}H NMR. Melting points were determined on a Tottoli melting point apparatus and are uncorrected. Thin-layer chromatography was carried out on Merck silica gel GF 254 plates; the following solvent systems were used: (A) *n*-butanol/H_2O/acetic acid (3:1:1); (B) chloroform/methanol (9:1); (C) chloroform/methanol/acetic acid (95:5:3).

Boc–D-Pro–Phe–OMe (III) (MW = 376.45). To a stirred and cooled (−15 °C) solution of Boc–D-Pro–OH (6.5 g, 30 mmol) in anhydrous $CHCl_3$/DMA (75 mL, 2 + 1), subsequently, 1 equiv of NMM (3.3 mL, 30 mmol) and 1.1 equiv of isobutyl chloroformate (4.27 mL, 33 mmol) were added. After 30–45 min (−15 °C), a precooled solution of H–Phe–OMe·HCl (6.5 g, 30 mmol) in anhydrous $CHCl_3$/DMA (75 mL, 2 + 1) containing NMM (3.3 mL, 30 mmol) was added. The obtained reaction mixture maintained at −10 °C for 1 h was then allowed to warm to room temperature. After completion of the reaction (TLC control), the mixture was concentrated under reduced pressure (bath temperature 40–45 °C), taken up in ethyl acetate (30 mL), and cooled to 4 °C. The salts were filtered off, and the organic layer was subsequently washed with aqueous 1 N HCl, saturated $NaHCO_3$, and saturated NaCl solution

and finally dried with Na_2SO_4. After concentration under reduced pressure, the oily residue was taken up in $CHCl_3$ and crystallization was initialized by adding dropwise petroleum ether (50–70 °C), producing white crystals (7.9 g, 70%). Mp: 106–107 °C. $[\alpha]_D^{20}$: 40.9° (*c* 1 in methanol). R_f: A, 0.77; B, 0.67; C, 0.69. ^{1}H NMR (DMSO-d_6): two sets of signals according to the two rotamers of the urethane NH–CO bond; 8.33 + 8.2 (each d, 1 H, Phe-NH); 7.16–7.33 (m, 5 H, aromatic protons); 4.6 (m, 1 H, Phe-α); 4.05 (m, 1 H, Pro-α); 3.66 + 3.61 (s, 3 H, OMe); 3.13–3.33 (m, 2 H, Pro-δ); 3.08 + 2.9 (each m, 2 H, Phe-β); 1.8–2.02, 1.63–1.73, 1.35–1.5 (each m, 4 H, Pro-β and -γ); 1.4 + 1.3 (each s (2 + 1), 9 H, tBu) ppm.

H–D-Pro–Phe–OMe·TFA (IV) (MW = 390.36). To a stirred solution of III (8 g, 21.24 mmol) in anhydrous CH_2Cl_2 (32 mL), TFA (32 mL) was added dropwise and the reaction mixture stirred for 30 min. The solution was concentrated under reduced pressure (bath temperature below 40 °C) and coevaporated with toluene (twice, 30 mL) and acetone (30 mL). The oily residue was taken up in a small amount of diethyl ether and crystallized by adding petroleum ether (50–70 °C). After drying in vacuo with KOH, a white amorphous solid was obtained (7.77 g, 93.7%). Mp: 127–129 °C. $[\alpha]_D^{20}$: 21.35 (*c* 1 in methanol). R_f: A, 0.53; B, 0.31; C, 0.23. ^{1}H NMR (DMSO-d_6): 9.08 (br, 2 H, NH_2^+); 7.15–7.35 (m, 5 H, aromatic protons); 4.65 (m, 1 H, Phe-α); 4.19 (m, 1 H, Pro-α); 3.68 (s, 3 H, OMe); 3.05–3.21 (m, 3 H, Pro-δ + one Phe-β); 2.89 (m, 1 H, second Phe-β); 2.13 + 1.42 (each m, 2 H, Pro-γ); 1.79 + 1.63 (each m, 2 H, Pro-β) ppm.

Z–Phe–D-Pro–Phe–OMe (V) (MW = 557.65). Z–Phe–OH (1.38 g, 4.55 mmol) and IV (1.38 g, 4.5 mmol) were dissolved in anhydrous THF (24 mL) containing NMM (0.55 mL, 5 mmol). The solution was cooled to −10 °C and subsequently mixed with HOBt (0.61 g, 4.5 mmol, EDCI·HCl (1.13 g, 5.85 mmol) and NMM (0.55 mL, 5 mmol). After stirring for 1 h at −10 °C, the mixture was warmed to room temperature and the reaction continued until completion (TLC control). The solution was concentrated under reduced pressure (bath temperature below 45 °C), taken up in ethyl acetate (35 mL), and cooled to 4 °C. The salts were filtered off, and the organic layer was subsequently washed with aqueous 1 N HCl, saturated $NaHCO_3$, and saturated NaCl solution and finally dried with Na_2SO_4. After concentration under reduced pressure to a volume of ca. 8 mL, diethyl ether/petroleum ether (1 + 10) was added until the solution became cloudy. Rapid crystallization took place, and the obtained product was dried in vacuo over P_2O_5, leaving a white amorphous solid (2.28 g, 91%). Mp: 121–122 °C. $[\alpha]_D^{20}$: 59.44° (*c* 1 in methanol). R_f: A, 0.87; B, 0.73; C, 0.68. ^{1}H NMR (DMSO-d_6): two sets of signals according to the two rotamers of the urethane NH–CO bond; 8.78, 7.96, 7.74 (each d, 2 H, NH signals); 7.1–7.35 (m, 15 H, aromatic protons); 4.93 (dd), 4.91 (s), (2 H, CH_2–Z group); 4.78, 4.45, 4.21, 4.04, 3.91 (each m, 3 H, α-protons); 3.6 (s, 3 H, OMe); 3.3 + 3.58 (each m, 2 H, Pro-δ); 2.68–3.2 (2 × dd, 4 H, all Phe-β); 2.03, 1.45–1.73, 1.4 (each m, 4 H, Pro-β and -γ) ppm.

Z–Phe–D-Pro–Phe–N_2H_3 (VI) (MW = 557.65). V (4 g, 7.16 mmol) was dissolved in absolute methanol (22 mL) and hydrazine monohydrate (7 mL, 143.6 mmol) added with stirring. After 10 h, the resulting suspension was concentrated under reduced pressure and further coevaporated with toluene (25 mL, six times) to remove excess hydrazine. The solid residue was dissolved in methanol and treated with water under stirring. The obtained amorphous solid was dried under vacuum over P_2O_5 (3.73 g, 93%). Mp: 111–113 °C. $[\alpha]_D^{20}$: 35.49 (*c* 0.8 in methanol). R_f: A, 0.78; B, 0.49; C, 0.44. ^{1}H NMR (DMSO-d_6): two sets of signals according to the two rotamers of the urethane NH–CO bond; 8.49 + 8.0 (each d, 1 H, Phe^3-NH); 7.68 + 7.62 (each d, 1 H, Phe^1-NH); 7.08–7.38 (m, 15 H, aromatic protons); 4.84–5.05 (m, 2 H, CH_2–Z group); 4.82, 4.45 (each m, 2 H, $Phe^{1,3}$-α); 4.16 + 4.0 (each m, 1 H, Pro-α); 3.52 + 3.28 (each m, 2 H, Pro-δ); 2.48–3.18 (m, 4 H, all Phe-β); 1.2–2.05 (m, 4 H, Pro-β and -γ); 8.9 and 4.1–4.4 (hydrazide), ppm.

Z–Glu(OtBu)–Phe–OMe (VII) (MW = 498.57). Z–Glu(OtBu)–OH·DCHA (2.18 g, 3.77 mmol) was dissolved in ethyl acetate (20 mL) and 20% aqueous solution of citric acid (10 mL) added. The two-phase system was stirred vigorously and then separated. The organic layer was concentrated under reduced pressure, and the oily residue was dried in vacuo over P_2O_5. The dried Z–Glu(OtBu)–OH was dissolved in anhydrous THF/DMA (20 mL, 1 + 1) and cooled to −15 °C. NMM (0.46 mL, 4.15 mmol) and isobutyl chloroformate (0.54 mL, 4.15 mmol) were added, and the mixture was stirred for 30 min at −15 °C. A solution of H–Phe–OMe/*p*-TsOH (1.32 g, 3.77 mmol) in anhydrous THF (20 mL) containing NMM (0.46 mL, 4.15 mmol) was cooled to −15 °C and added to the reaction mixture. After 1 h of stirring at −10 °C, the solution was allowed to warm to room temperature. Stirring was continued until completion of the reaction (TLC control): The reaction mixture was concentrated in vacuo and taken up in ethyl acetate (30 mL). The suspension was cooled to 4 °C, the salts were filtered off, and the organic layer was subsequently extracted with aqueous 1 N HCl, saturated $NaHCO_3$, and saturated NaCl solution and then dried with Na_2SO_4. The ethyl acetate layer was concentrated to a volume of 10 mL. Dropwise addition of isohexane with stirring afforded crystallization of the desired product (1.05 g, 55.6%). Mp: 82–85 °C. $[\alpha]_D^{20}$: −12.68° (*c* 0.9 in methanol). R_f: A, 0.85; B, 0.68; C, 0.73. ^{1}H NMR (DMSO-d_6): 8.29 (d, 1 H, Phe-NH); 7.28 (d, 1 H, Glu-NH); 7.13–7.43 (m, 10 H, aromatic protons); 5.02 (s, 2 H, CH_2–Z group); 4.48, 4.02 (each m, 2 H, α-protons); 3.59 (s, 3 H, OMe); 3.0 (2 × dd, 2 H, Phe-β); 2.18 (m, 2 H, Glu-γ); 1.6–1.9 (m, 2 H, Glu-β); 1.39 (s, 9 H, OtBu) ppm.

Z–Ala–Glu(OtBu)–Phe–OMe (VIII) (MW = 569.65). A solution of VII (1.6 g, 3.2 mmol) in anhydrous methanol (40 mL) was hydrogenated with Pd 10% on charcoal (400 mg) as catalyst under standard procedure. After completion of the reaction (TLC control eluent B, R_f(product) 0.7), the catalyst was filtered off and the organic layer evaporated. The oily residue was coevaporated with toluene (twice, 30 mL) and used for coupling without further purification. Z–Ala–OH (692 mg, 3.1 mmol) and NMM (0.45 mL, 3.5 mmol) were dissolved in anhydrous THF (10 mL) and cooled to −15 °C, and isobutyl chloroformate (0.44 mL, 3.4 mmol) was added. The reaction mixture was stirred for 30 min at −10 °C, the cooled solution of the above hydrogenation product in anhydrous DMA (15 mL) was added, stirred for 1 h, and allowed to warm to room temperature, and after completion of the reaction (TLC control) the solution was concentrated under reduced pressure. The residue was taken up in $CHCl_3$ (30 mL), and the organic layer was subsequently washed with aqueous 1 N HCl, saturated $NaHCO_3$, and saturated NaCl solution. Further concentration to 6 mL volume and addition of isohexane afforded crystallization of the product as a white solid (1.52 g, 86%). Mp: 138–139 °C. $[\alpha]_D^{20}$: −26.6° (*c* 0.6 in methanol). R_f: A, 0.67; B, 0.67; C, 0.64. ^{1}H NMR (DMSO-d_6): 8.3, 7.88 (each d, each 1 H, Phe,Glu-NH); 7.45 (d, 1 H, Ala-NH); 7.12–7.45 (m, 10 H, aromatic protons); 5.01 (s, 2 H, CH_2–Z group); 4.48, 4.29, 4.05 (each m, each 1 H, α-protons); 3.59 (s, 3 H, OMe); 3.0 (2 × dd, 2 H, Phe-β); 2.2 (m, 2 H, Glu-γ); 1.5–1.95 (m, 2 H, Glu-β); 1.38 (s, 9 H, OtBu); 1.15 (d, 3 H, Ala-CH_3) ppm.

Z–Phe–D-Pro–Phe–Ala–Glu(OtBu)–Phe–OMe (IX) (MW = 961.12). A solution of VIII (1.3 g, 2.28 mmol) in anhydrous methanol (50 mL) was hydrogenated with Pd 10% on charcoal (290 mg) as catalyst under standard procedures. After completion of the reaction (TLC control eluent B, R_f(product) 0.7), the catalyst was filtered off and the organic layer evaporated. The oily residue was coevaporated with toluene (twice, 30 mL) and used for coupling without further purification. VI (1.26 g, 2.25 mmol) was dissolved in anhydrous DMA (13 mL) and cooled to −20 °C. HCl (36% in water, 0.9 mL, 5 mol equiv) was carefully added and the solution cooled to −20 °C before isopentyl nitrite (0.5 mL, 3.71 mmol) was quickly added. The reaction mixture was kept dry and dark with stirring for 1.5 h at −10 °C, and then the precooled solution of the above hydrogenation product in anhydrous DMA (10 mL) containing DIPEA (3.5 mL, 20.41 mmol) was added (resulting pH of the solution 7.5–8). After standing for 12 h at 4 °C, the reaction mixture was concentrated under reduced pressure and the resulting residue was taken up in $CHCl_3$ (50 mL). Subsequent washing of the organic layer with aqueous 1 N HCl, saturated $NaHCO_3$, and saturated NaCl solution afforded after evaporation of the organic layer a crude product that could be recrystallized from methanol by addition of water (2 g, 92.5%). Mp: 104–105 °C. $[\alpha]_D^{20}$: 4.4° (*c* 0.4 in DMF). R_f: A, 0.68; B, 0.78; C, 0.67. ^{1}H NMR (DMSO-d_6): two sets of signals according to the two rotamers of the urethane NH–CO bond.

Cyclo[-D-Pro^1–Phe^2–Ala^3–Glu(OtBu)^4–Phe^5–Phe^6–] (II) (MW = 794.95). The fully protected hexapeptide IX (1.5 g, 1.56 mmol) was dissolved in anhydrous methanol (19 mL) and stirred with hydrazine monohydrate (1.53 mL, 31.2 mmol) for 16 h. The resulting suspension was evaporated and further coevaporated with toluene (30 mL, 3–4 times) to remove excess hydrazine. The crude product was suspended in methanol/acetic acid (50 mL, 2 + 1) and hydrogenated with Pd 10% on charcoal (300 mg, dried) as catalyst. After completion of the reaction (TLC control eluent B), the now clear solution was filtered and concentrated to dryness. The crude product was dried over P_2O_5 under vacuum; it showed no more signal for protecting groups in NMR spectra. The deprotected hexapeptide was dissolved in anhydrous DMF (11.5 mL) and cooled to −20 °C. After careful addition of HCl (36% in water, 0.58 mL, 7.23 mmol), isopentyl nitrite (0.32 mL, 2.39 mmol) was added. The reaction stood dry and dark at −10 °C for 1.5 h. The reaction mixture was added to a stirred and cooled (−18 °C) vessel containing 2 L of anhydrous DMF. The pH of the solution was adjusted to 7.5–8 by adding DIPEA (ca. 8 mol equiv, 3.72 mL) and stored for 5 days at 4 °C. The organic layer was evaporated (bath temperature below 45 °C) and the oily residue taken up in methanol/water (60 mL, 5 + 1) and shaked with ion exchange resin (Merck-Mischbett, 15 g). The layer was evaporated in vacuo and the resulting residue recrystallized from $CHCl_3$/diethyl ether. The obtained amorphous solid was subsequently treated

Table XI. 250-MHz ^1H and 75-MHz ^{13}C Chemical Shifts (ppm) of Cyclo(-D-Pro^1-Phe^2-Ala^3-[*N*-(2-acetamido-3,4,6-tri-*O*-acetyl-2-desoxy-β-D-glucopyranosyl)]Gln^4-Phe^5-Phe^6-) in DMSO-d_6 at 300 K[a]

	Phe^6	D-Pro^1	Phe^2	Ala^3	Gln^4	Phe^5
NH	7.27	-	8.75	7.88	8.12	8.01
Hα	4.63	4.09	4.22	4.45	3.55	4.32
Hβ	3.10	1.66	3.22	1.49	1.79	3.20
	2.78	1.47	2.73	-	1.61	3.03
Hγ	-	1.86[b]	-	-	2.07	-
Hδ	-	3.33	-	-	-	-
	-	2.72	-	-	-	-
aromatic protons, 7.40–7.10; acetyl protons, 2.01, 1.98, 1.94						
Cα	53.1	59.7	54.4	47.1	55.9	54.4
Cβ	39.8	28.2	35.8	18.3	25.6	36.4
Cγ	-	24.5	-	-	31.4	-
Cδ	-	46.7	-	-	-	-
carbonyls, 172.3–168.5 aromatic protons, 138.7–126.1; acetyl, 20.5–20.3						

[a] GlcNAc (^1H NMR): 8.42 (d, 1 H, N^{1}H), 7.98 (d, 1 H, N^{2}H), 5.18 (m, 1 H, H-1), 5.12 (m, 1 H, H-3), 4.81 (m, 1 H, H-4), 4.20 u. 3.95 (m, 1 H, H-6), 3.85 (m, 1 H, H-2), 3.82 (m, 1 H, H-5), 1.78 (s, 3 H, CH_3-NHAc). GlcNAc (^{13}C NMR): 77.9 (C-1), 73.3 (C-3), 72.2 (C-5), 68.4 (C-4), 61.8 (C-6), 52.2 (C-2), 22.6 (CH_3-NHAc). [b] Both diastereotopic protons.

with aqueous saturated $NaHCO_3$ and 0.5 N HCl solution and water, giving after drying in vacuo the pure product (1.0 g, 80.6%). Mp: 116–118 °C. $[\alpha]_D^{20}$: −43.92° (*c* 0.5 in methanol). R_f: A, 0.79; B, 0.58; C, 0.54. FAB-MS: *m/e* 795 (M + H$^+$). NMR data are given in Table I.

Cyclo[-D-Pro^1-Phe^2-Ala^3-Glu^4-Phe^5-Phe^6-] (X) (MW = 738.84). The cyclic hexapeptide VIII (300 mg, 0.377 mmol) was stirred in an ice cold solution of HCl_{gas} in diethyl ether (90 mL) for 30 min. The organic layer was evaporated and the white solid residue coevaporated with toluene (30 mL, twice). The product was dried over KOH under vacuum, giving white crystals (277 mg, quantitative). Mp: 137–138 °C. $[\alpha]_D^{20}$: −43.38 (*c* 0.8 in methanol). R_f: A, 0.8; B, 0; C, 0.06.

Cyclo(-D-Pro^1-Phe^2-Ala^3-[*N*-(2-acetamido-3,4,6-tri-*O*-acetyl-2-desoxy-β-D-glucopyranosyl)]Gln^4-Phe^5-Phe^6-) (XI) (MW = 1067.16). To a cooled (−15 °C) stirred solution of cyclo(-D-Pro^1-Phe^2-Ala^3-Glu^4-Phe^5-Phe^6-) (0.122 mmol, 90 mg) in anhydrous THF (2 mL), subsequently HOBt (2 equiv, 0.244 mmol, 38 mg) and EDCI (2 equiv, 0.244 mmol, 47 mg) were added. After 1 h, 2-acetamido-3,4,6-tri-*O*-acetyl-2-desoxy-β-D-glucopyranosylamine (3 equiv, 0.366 mmol, 127 mg) was added and the reaction mixture maintained for 1 h at −15 °C and then allowed to warm to room temperature. After 3 days, EDCI (2 equiv, 0.244 mmol, 47 mg) and 2-acetamido-3,4,6-tri-*O*-acetyl-2-desoxy-β-D-glucopyranosylamine (2 equiv, 0.244 mmol, 85 mg) were added at 0 °C for completion of the reaction. When the reaction was finished (TLC control, 5 days), the mixture was concentrated in vacuo (bath temperature below 30 °C), taken up in ethyl acetate, and subsequently washed with aqueous 1 N HCl, saturated $NaHCO_3$, and saturated NaCl solution. The organic layer was dried (Na_2SO_4) and concentrated. Chromatography of the obtained residue with silica gel 60 (70–230 mesh ASTM) in chloroform/2-propanol (10:1), evaporation of the solvent, and drying over P_2O_5 afforded the product as an amorphous white solid (83 mg, 64%). $[\alpha]_D^{20}$: −27.5° (*c* 0.6 in methanol). R_f: A, 0.76; B, 0.33; C, 0.09; $CHCl_3$/2-propanol (10:1), 0.13. FAB-MS: *m/e* 1067.5 (M + H$^+$), 1089.5 (M + Na$^+$). 250-MHz ^1H and 75-MHz ^{13}C chemical shifts (ppm) of cyclo(-D-Pro^1-Phe^2-Ala^3-[*N*-(2-acetamido-3,4,6-tri-*O*-acetyl-2-desoxy-β-D-glucopyranosyl)]Gln^4-Phe^5-Phe^6-) in DMSO-d_6 at 300 K are given in Table XI.

Cyclo(-D-Pro^1-Phe^2-Ala^3-[*N*-(2-acetamido-2-deoxy-β-D-glucopyranosyl)]Gln^4-Phe^5-Phe^6-) (I) (MW = 941.05). Cyclo(-D-Pro^1-Phe^2-Ala^3-[*N*-(2-acetamid-3,4,6-tri-*O*-acetyl-2-desoxy-β-D-glucopyranosyl)]Gln^4-Phe^5-Phe^6-) (0.0328 mmol, 35 mg) was coevaporated with toluene and dissolved in anhydrous methanol/ethanol (1:1, 1 mL). After addition of KCN (0.6 equiv, 0.0197 mmol, 1.3 mg; dried by coevaporation with toluene and applied as a solution in anhydrous methanol/ethanol (1:1, 1 mL)), the reaction was stirred in an argon atmosphere at room temperature until the reaction was completed (TLC control, 12 h). The mixture was filtered directly through a short column filled with silica gel 60, eluted with ethanol, and concentrated. Purification by HPLC (Nucleosil C18/10λ, chloroform/2-propanol (1:1)), evaporation, and drying over P_2O_5 yielded the product as an amorphous white solid (25 mg, 81%). $[\alpha]_D^{20}$: −24.0° (*c* 0.9 in methanol). R_f: chloroform/2-propanol (1:1), 0.34.

b. NMR Measurements. All spectra were recorded on a Bruker AMX600 spectrometer, with the exception of the E.COSY (Bruker AC250 spectrometer) and the HMBCS (Bruker AMX500 spectrometer). The samples contained 10.0 mg of I and 30.0 mg of II, respectively, in 0.5 mL of DMSO-d_6 (99.9% ^2H atoms; Aldrich). All chemical shifts are referenced to the DMSO-d_6 signal at 2.5 ppm for ^1H and 39.5 ppm for ^{13}C.

(1) 1D ^1H NMR spectra: size 16 K, pulse length 3.0 μs, 80 acquisitions. The spectra for determination of the temperature gradients were recorded at 300–340 K in steps of 10 K for I and II.

(2) DQF-COSY spectra: sequence D_1–90°–t_1–90°–D_2–90°–t_2, relaxation delay D_1 = 1.3 s, D_2 = 4 μs, 90° pulse 7.8 μs, spectral width in both dimensions f_1 and f_2 7142.8 Hz, quadrature detection in both dimensions.

(3) NOESY spectra: sequence D_1–90°–t_1–90°–τ_{mix}–90°–t_2, relaxation delay D_1 = 1.3 s, mixing time τ_{mix} 120 ms, no random variation of τ_{mix}, 90° pulse 7.8 μs, spectral width in both dimensions f_1 and f_2 7142.8 Hz, quadrature detection in both dimensions.

(4) TOCSY spectra: sequence D_1–90°–t_1–MLEV17–t_2, relaxation delay D_1 = 1.3 s, spectra with different mixing times (duration of the spin-lock period) were recorded (a, 20 ms; b, 80 ms), 90° pulse 7.8 μs, spectral width in both dimensions f_1 and f_2 7142.8 Hz, quadrature detection in both dimensions.

(5) ROESY spectra: sequence D_1–90°–t_1–$(P_5$–$D_3)_n$–t_2, relaxation delay D_1 = 1.3 s, D_3 = 20.5 μs, 90° pulse 7.8 μs, P_5 pulse for spin-lock field 2 μs, mixing time 120 μs, spectral width in both dimensions f_1 and f_2 7142.8 Hz, quadrature detection in both dimensions.

(6) E.COSY spectra: sequence D_1–90°–t_1–90°–D_2–t_2, phase cycling according to ref 38, relaxation delay D_1 = 1.3 s, D_2 = 3 μs, 90° pulse 7.1 μs, spectral width in both dimensions f_1 and f_2 2000.0 Hz, quadrature detection in both dimensions.

(7) Proton-detected ^1H, ^{13}C-COSY (HMQC) spectra (600 MHz): sequence D_1–BIRD–D_4–90°(^1H)–D_2–90°(^{13}C)–t_1/2–180°(^1H)–t_1/2–90°(^{13}C)–D_2–t_2(GARP[^{13}C]), relaxation delay D_1 = 197 ms, D_2 = 3.57 ms, D_4 = 117 ms, 90° pulse (^1H) 12.5 μs, 90° pulse (^{13}C) 10.4 μs, spectral width in f_2 5434.78 Hz (=9.056 ppm) and f_1 11 363.64 Hz (=75.3 ppm), quadrature detection in both dimensions, recording and processing in the phase-sensitive mode.

(8) "Inverse COLOC" with 270° Gaussian pulse (HMBCS) spectra: sequence D_1–90°(^1H)–D_4–270°$_{selective}$(^{13}C)–t_1/2–180°(^1H)–t_1/2–90°(^{13}C)–t_2, relaxation delay D_1 = 2.0 s, 90° pulse (^1H) 7.8 μs, 90° pulse (^{13}C *hard*) 12.4 μs, 270° pulse (^{13}C *soft*) 2000 μs, D_4 = 50 ms, spectral width in f_2 5555.56 Hz, in f_1 140.0 Hz, the spectra were phase-sensitively recorded and processed, followed by a magnitude calculation in f_2.

(9) Proton-detected ^1H, ^{13}C-COSY with TOCSY transfer (HMQC-TOCSY) spectra: sequence D_1–BIRD–D_4–90°(^1H)–D_2–90°(^{13}C)–t_1/2–180°(^1H)–t_1/2–90°(^{13}C)–D_2–MLEV17–t_2(GARP[^{13}C]), relaxation delay D_1 = 197 ms, D_2 = 3.57 ms, D_4 = 117 ms, 90° pulse (^1H) 12.5 μs, 90° pulse (^{13}C) 10.4 μs, spectral width in f_2 5434.78 Hz (=9.056 ppm) and f_1 11 363.64 Hz (=75.3 ppm), mixing time for the spin lock 80 ms, quadrature detection in both dimensions, recording and processing in the phase-sensitive mode.

(10) HMQC-NOESY-spectrum: sequence D_1–BIRD–D_4–90°(^1H)–D_2–90°(^{13}C)–t_1/2–180°(^1H)–t_1/2–90°(^{13}C)–D_2–90°(^1H)–τ_{mix}–90°(^1H)–t_2(GARP[^{13}C]), relaxation delay D_1 = 235 ms, D_2 = 3.57 ms, D_4 = 225 ms, 90° pulse (^1H) 12.5 μs, 90° pulse (^{13}C) 10.4 μs, spectral width in f_2 5434.78 Hz (=9.056 ppm) and f_1 11 363.64 Hz (=75.3 ppm), mixing time for the NOE transfer step 200 ms, quadrature detection in both dimensions, recording and processing in the phase-sensitive mode, coadded rows of a spectral region without cross peaks were subtracted from the 2D matrix.

Acknowledgment. We are indebted to Mrs. Ellen Lichte for several HPLC purifications of the described compounds. Financial support by the Deutsche Forschungsgemeinschaft and the Fonds der chemischen Industrie is gratefully acknowledged. We thank Prof. Dr. W. F. van Gunsteren and Dr. A. E. Torda for the GROMOS package and helpful discussions, Dr. H. W. Fehlhaber (Hoechst AG) for the mass spectra, Thomas Wein for help in performing the calculations, and Dr. D. F. Mierke for his careful reading of the paper. M.K. and H.M. thank the Fonds der chemischen Industrie for a fellowship.

Registry No. I, 135512-68-4; II, 135481-61-7; III, 74086-60-5; IV, 135481-63-9; V, 135481-64-0; VI, 135481-65-1; VII, 53119-74-7; VIII, 135481-66-2; IX, 135481-67-3; X, 135481-68-4; XI, 135481-69-5; H-Phe-OMe·HCl, 7524-50-7; BOC-D-Pro-OH, 37784-17-1; Z-Phe-OH, 1161-13-3; Z-Glu(OtBu)-OH·DCHA, 3967-21-3; Z-Glu(OtBu)-OH, 3886-08-6; H-Phe-OMe·*p*-TsOH, 67436-23-1; H-Glu(OtBu)-Phe-OMe,

135481-70-8; Z-Ala-OH, 1142-20-7; H-Ala-Glu(OtBu)-Phe-OMe, 135481-71-9; H-Phe-D-Pro-Phe-Ala-Glu(OtBu)-Phe-$NHNH_2$·2HOAc, 135481-73-1; 2-acetamido-3,4,6-tri-*O*-acetyl-2-deoxy-β-D-glucopyranosylamine, 4515-24-6.

Supplementary Material Available: Additional six figures (parts of 250-MHz E.COSY for I and II, part of the 600-MHz TOCSY spectrum of I, parts of the 600-MHz NOESY spectra of II (NH/C_α region) and I (NH/NH region), and expansion of the 600-MHz HMQC-NOESY spectrum (NH/C_α region)) (7 pages). Ordering information is given on any current masthead page.

The Influence of Altered Amidic Resonance on the Infrared and ^{13}C and ^{15}N NMR Spectroscopic Characteristics and Barriers to Rotation about the N–C(O) Bond in Some Anilides and Toluamides

A. J. Bennet,[†] V. Somayaji,[†] R. S. Brown,*[,†] and B. D. Santarsiero[‡]

Contribution from the Department of Chemistry, University of Alberta, Edmonton, Alberta, Canada, and Structure Determination Laboratory, Department of Chemistry, University of Alberta, Edmonton, Alberta, Canada. *Received January 22, 1991*

Abstract: In order to provide physicochemical evidence for or against amidic resonance, three series of anilides and toluamides have been investigated by infrared spectroscopy and ^{13}C and ^{15}N NMR, and barriers to rotation for several toluamides have been determined. Each series contains amides that are predisposed in one or more ways to disfavor resonance. These include rotation about the N–C(O) bond in a series of bicyclic anilides, N-pyramidalization in a series of *N*-toluoyl cyclic amines, and removal of N electron density in some toluamides by inductive means or by occupying the N lone pair in an aromatic sextet. The structures of the *N*-toluoyl derivatives of azetidine, pyrrole, and 2,5-dimethylpyrrole were determined by X-ray diffraction. The physicochemical data are generally consistent with the resonance model, but there are anomalies indicating that other factors are also important. When resonance is favored, the infrared $\nu_{C=O}$ and ν_{C-N} bands are respectively found at lower and higher values than in amides where resonance is disfavored. The ^{13}C NMR chemical shift for a wide variety of toluamides and anilides with different resonance abilities consistently appears between δ 167 and 172 ppm, except for the distorted bicyclic anilides (δ 180–200 ppm) or *N*-toluoylaziridine (δ 178 ppm). Since the sets include amides of considerable structural diversity, the $^{13}C{=}O$ chemical shifts are compared with the ^{13}C chemical shift of the corresponding *N*-methylamine: the $\Delta\delta(^{13}C)$(amide–amine) values span a range of ~122–143 ppm, with amides having inhibited resonance lying at the higher values. ^{15}N chemical shifts for amides for which resonance can be invoked appear to be ~80 ppm downfield from their corresponding N-methylated tertiary amines. The ^{15}N chemical shifts of amides in which resonance is impaired by rotation about the N–C(O) bond, by N-pyramidalization, or by occupying the N lone pair in an aromatic sextet move upfield by ~30–40 ppm, but are still 45–50 ppm downfield from their corresponding tertiary amines. The $\Delta G^{\ddagger}$ for rotation about the N–C(O) bond in a series of toluamides appears to be relatively insensitive to the ability of the N to support (+)-charge as gauged by the gas-phase basicity of the corresponding amines. Where structural and $\Delta G^{\ddagger}$ rotational data can be compared, those amides with short N–C(O) bonds (1.34–1.37 Å) have high rotational barriers (14.5–16.5 kcal/mol), while those amides with longer N–C(O) bonds (1.40–1.42 Å) have reduced barriers to rotation (<6–8 kcal/mol).

Resonance theory[1] has enjoyed applicability in explaining various properties of amides such as the short N—C(O) bond length,[2] planar geometry,[2] barrier to N—C(O) rotation,[3] C=O IR stretching frequencies,[4] ^{15}N NMR chemical shifts,[5] and kinetic stability toward nucleophilic attack/hydrolysis.[6] However, the importance of resonance contributor **1a** has been questioned by

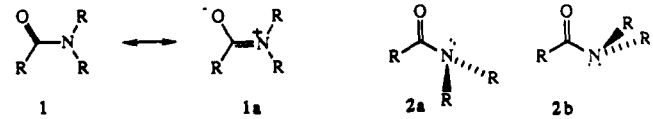

1 **1a** **2a** **2b**

Wiberg and Laidig[7] who have reported high-level ab initio calculations on planar and orthogonal formamides (**1**, **2**, R = H, respectively) along with Bader's electron population analysis[8] for the various atoms in each conformer. In contrast to what is expected on the basis of the resonance model, the computed electron population at N in **1**, R = H, is larger than in **2**, R = H, while the population at each O is similar. In **1**, the electron population at C is less than in **2** so that there is a net transfer of electrons from C to N in the former. The N—C(O) bond lengthens in passing from **1** to **2**, but the C=O bond length is scarcely affected. Finally, the computed barrier to N—C(O) rotation (**1** → **2b** → **1**) is similar to the experimental one of 18–19 kcal/mol.[9] Wiberg and Laidig,[7] Bader et al.[10a] and Wiberg and

[†] Department of Chemistry.
[‡] Structure Determination Laboratory, Department of Chemistry.

(1) Pauling, L. *The Nature of the Chemical Bond*; Cornell University Press: Ithaca, NY, 1940.
(2) a. Chakrabarti, P.; Dunitz, J. D. *Helv. Chim. Acta* **1982**, *65*, 1555. b. Vankatesan, K.; Ramakumar, S. In *Structural Studies of Molecular Biological Interest*; Dodson, G., Gluskar, J. P., Sayre, D., Eds.; Oxford University Press: New York, 1981; pp 137–153.
(3) a. Robin, M. B.; Bovey, F. A.; Basch, H. In *The Chemistry of Amides*; Zabicky, J., Ed.; Wiley-Interscience: London, 1970; pp 1–72. b. Stewart, W. E.; Siddall, T. H. *Chem. Rev.* **1970**, *70*, 517. c. Toriumi, Y.; Kasuya, A.; Itai, A. *J. Org. Chem.* **1990**, *55*, 259.
(4) a. Eglinton, G. In *An Introduction to Spectroscopic Methods for the Identification of Organic Compounds*; Scheinniann, F., Ed.; Pergamon Press: Oxford, 1990; Vol. 1., pp 123–143. b. Lambert, J. B.; Shurwell, H. F.; Verbit, L.; Cooks, R. G.; Stout, G. H. *Organic Structural Analysis*; MacMillan Publishing Co., Inc.: New York, 1976; pp 187–252. c. Silverstein, R. M.; Bassler, G. C.; Marrill, T. C. *Spectrometric Identification of Organic Compounds*, 4th ed.; J. Wiley and Sons: New York, 1981; pp 117–127.
(5) a. Levy, G. C.; Lichter, R. L. *Nitrogen-15 Nuclear Magnetic Resonance Spectroscopy*; J. Wiley and Sons: New York, 1979; pp 58–67. b. Witanowski, M.; Stefaniak, L.; Webb, G. A. *Annu. Rep. NMR Spectrosc.* **1986**, *18*, 1.
(6) Deslongchamps, R. *Stereoelectronic Effects in Organic Chemistry*; Pergamon Press: Oxford, 1983; pp 101–162.
(7) Wiberg, K. B.; Laidig, K. E. *J. Am. Chem. Soc.* **1987**, *109*, 5935.
(8) Bader, B. F. W.; Nguyen-Dang, T. T. *Adv. Quantum Chem.* **1981**, *14*, 63.

0002-7863/91/1513-7563$02.50/0